UNIVERSITAT DE BARCELONA

Departament d'Astronomia i Meteorologia

Astrophysical Studies on Open Clusters:

NGC 1807, NGC 1817, NGC 2548 and NGC 2682

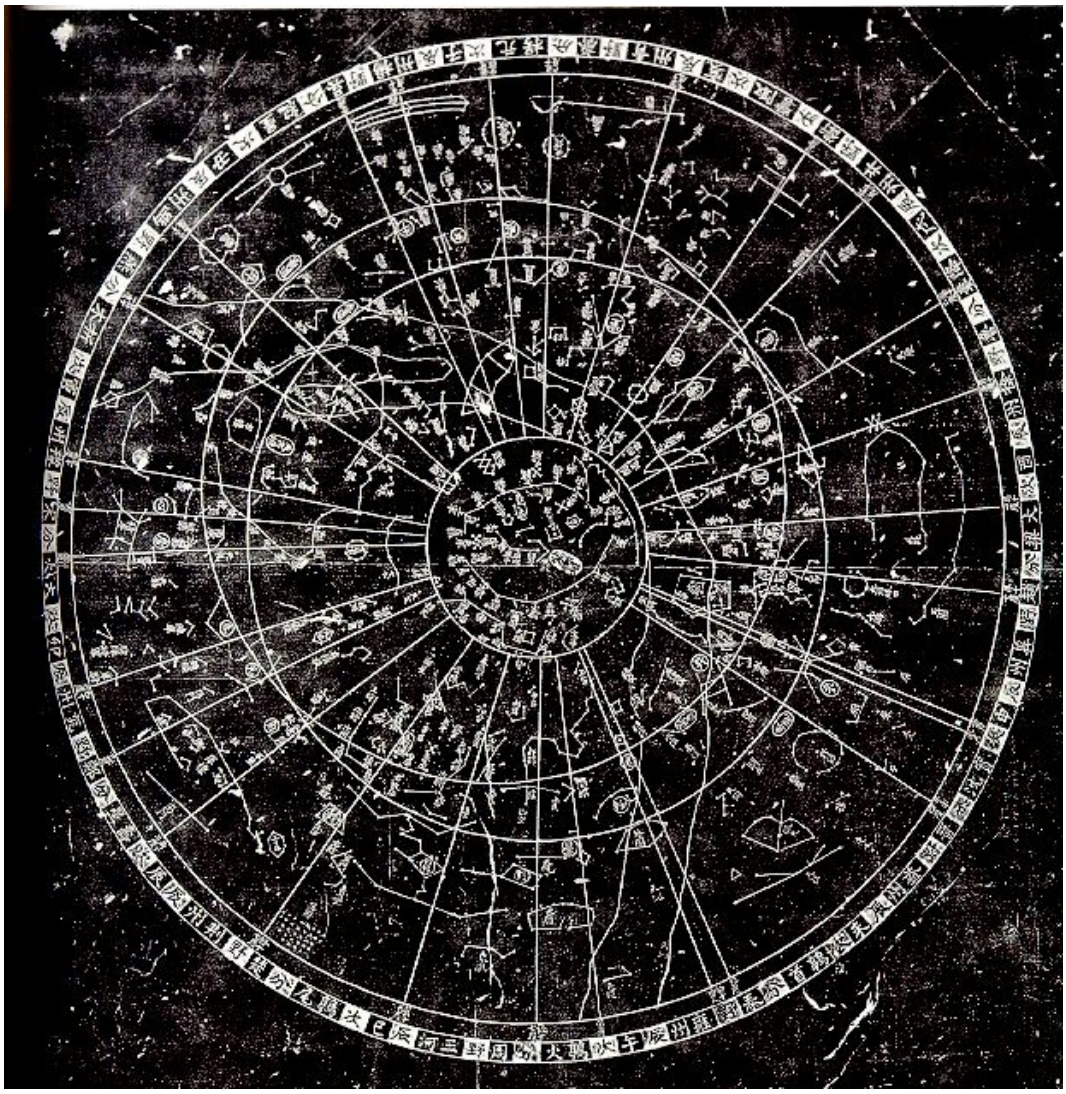

Memoria presentada por

María de los Dolores Balaguer Núñez

para optar al grado de

Doctora en Física

Barcelona, 31 de octubre de 2005

登幽州台歌

前不見古人，
後不見來者；
念天地之悠悠，
獨愴然而涕下。

陳子昂 (658-699)

Upon Ascending the Parapet at Youzhou[a]

Before me, unseen are the ancients,
behind me, unseen those to come.
Thinking of this infinite universe,
Alone, in my sorrow, I shed tears.

Chen Ziang (661 - 702)

[a]Translated by Wilson & Zhang (1995)

2 NGC 1817 and NGC 1807: Proper motions and membership probabilities

Proper motions of some stars in the region of NGC 1817 and NGC 1807 were first published by Li (1954) based on plates taken with the 40 cm astrograph at Shanghai Zŏ-Sè station. The accuracy of its proper motions is rather low since the epoch difference of the plates used was only twelve years. Later on, in 1980's also at Shanghai Observatory, three pairs of plates of the NGC 1817/NGC 1807 area were measured manually on the Zeiss Ascorecord measuring machine at Zŏ-Sè. Relative proper motions in the cluster region were obtained from these plate measurements, and its membership determination was made (Tian et al. 1983). These proper motions are not very accurate because of manual measuring. No other astrometric study exists of the area.

For the present work, six more plates were taken at the same Observatory and all available plates were, for first time, measured automatically. A first study[1] of the area determined accurate relative proper motions of 722 stars within a $1\overset{\circ}{.}5 \times 1\overset{\circ}{.}5$ area in the NGC 1817/NGC 1807 region. Through estimating membership probabilities with an improved likelihood method for two clusters in the area (Tian et al. 1998), the membership determination led us to distinguish two separate clusters in the region, with different distribution parameters: NGC 1817 and NGC 1807. For the reasons explained in Section 2.5, we decided to improve our results and a second study[2] leaded to accurate absolute proper motions of 810 stars in the area. A new

[1]Sections 2.1-2.4 are based on: Balaguer-Núñez L., Tian K.P., & Zhao J.L., 1998, A&AS 133, 387

[2]Sections 2.5-2.7 are based on: Balaguer-Núñez L., Jordi C., Galadí-Enríquez D., & Zhao J.L.,

membership determination using parametric and non-parametric approaches was applied and the distribution parameters of only one cluster obtained.

2.1 Plate material and measurements

Twenty-five plates of the NGC 1817/NGC 1807 region are available. They were taken with the double astrograph at the Zô-Sè station of Shanghai Observatory. This telescope has an aperture of 40 cm, a focal length of 6.9 m and hence a plate scale of $30''$ mm^{-1}. The size of the plates is 24 cm by 30 cm, or $2\overset{\circ}{.}0 \times 2\overset{\circ}{.}5$. Although the plates cover quite a wide sky area, only a section of $1\overset{\circ}{.}5 \times 1\overset{\circ}{.}5$ around the cluster centre was measured for this study. The oldest plate was taken in 1916, and the most recent ones in 1997 explicitely for this PhD work. The relevant information on these plates is given in Table 2.1.

All the plates were measured on a Photometric Data Systems (PDS) model 1010 automatic measuring machine at the Purple Mountain Observatory in Nanjing (China). The high precision measurements of astrometric plates were performed in two steps. First, the rough coordinates of the star images to be measured were obtained with a full area scan in high speed. Next, the high precision measurements of these images were obtained with a image-by-image fine scan by means of the rough coordinates in lower speed. There is a total of 916 stars being measured with a photographic magnitude limit close to about 15.0. An aperture size of 20 by 20 microns, scanning step of 20 μm, scanning speed of 25 μm s^{-1} and R scanning type were adopted. All the scanning programs were provided by J.J. Wang and explained in Wang et al. (1990); Wang & Chen (1992); Wang (1994, 1995). In order to monitor and reduce any possible plate displacements and the resulting systematic errors, all the stellar images to be measured were divided into 18 groups, all the groups sharing four common images which were scanned twice, before and after all the other images for each group. Program PDSGRC was used to examine the stability of grouping measurements, in order to reduce both the errors due to plate displacements mentioned above and, if necessary, those arising from plate rotation and/or expansion/contraction. The program for digital image centring (PDSDIC) is based on the algorithm developed by Lee & van Altena (1983). Since the profiles of seeing-limited stellar images are nearly Gaussian, a density array, D_{ij}, around each

Table 2.1: Shanghai Observatory (Zô-Sè astrograph) plates of NGC 1817/NGC 1807 area.

Plate id.	Epoch (1900+)	Exp.time min:sec	N. of stars
CL415	16.01.31	30	159
CL5293	30.02.16	–	660
CL5291	43.02.09	–	537
CL5292	43.02.22	–	634
CL54002	54.01.31	80	684
CL54003	54.02.08	90	656
CL61010	61.02.02	40	848
CL61003	61.02.12	20	602
CL61002	61.02.17	30	714
CL81009	81.12.24	20	464
CL81010	81.12.24	20	508
CL81011	81.12.25	15	588
CL81012	81.12.25	15	512
CL82001	82.02.24	15	701
CL82002	82.02.24	15	678
CL82003	82.02.24	12	655
CL82004	82.02.27	8:15	606
CL82005	82.02.27	5:45	373
CL82006	82.02.27	15	651
P9701	97.01.02	30	470
P9702	97.01.11	30	426
P9703	97.01.11	30	478
P9704	97.01.11	30	168
P9705	97.01.12	30	587
P9706	97.01.12	30	540

image can be modelled by a two-dimensional five-parameters Gaussian function:

$$F(x,y) = D_0 \exp\left(\frac{-r^2}{2R^2}\right) + b, \tag{2.1}$$

$$r^2 \ = (x-x_0)^2 + (y-y_0)^2. \tag{2.2}$$

The centre (x_0, y_0) represents the position of the star. The image radius R and the peak density D_0 are related to the magnitude of the star, while b gives the surrounding sky background. These parameters can be determined from a Gaussian fit to the density array marginal distribution $F(x,y)$.

2.2 Relative proper motions: plate-pair technique

The reduction of the relative proper motions for 722 stars in the region of NGC 1817 and NGC 1807 was made on the basis of the PDS measurements by means of an approach adopted many times before (Tian et al. 1982, 1983; Zhao et al. 1993, 1980; Su et al. 1998). There are three steps in the whole process: the first is to transform the measured positions for all stars in all the plates to a common system, in order to eliminate the errors due to small differences in the orientation of different plates in scanning; the second step is to establish a reference frame, i.e. to decide upon the reference stars; the last step is to calculate proper motions of all the stars with respect to this reference frame, and their corresponding uncertainties.

After two loops of a least-squares adjustment, 83 stars with residuals in both x and y coordinates less than $2\sigma_{\mu_x}$ and $2\sigma_{\mu_y}$, respectively, were chosen to be reference stars from the 99 stars common to all the plate pairs, where σ_{μ_x} and σ_{μ_y} are the r.m.s. residuals in the x and y coordinates obtained from the least-squares adjustment. This defines a preliminary proper motion system in which the proper motions of the selected stars are collectively free of translation, rotation and expansion.

Owing to the limited number of reference stars and the precision of their proper motions, the plate pair technique was used in this case. The information of the plate pairs used is given in Table 2.2. All the linear and quadratic coordinate-dependent terms and the coma term are included in the plate solutions:

$$x' = a_0 + a_1 x + a_2 y + a_3 x^2 + a_4 xy + a_5 y^2 + a_6 mx \tag{2.3}$$

Table 2.2: Plate-pairs material

Pair No.	Plate id.	Epoch (1900+)	Exp.Time min:sec	Baseline years	N. of Stars
1	CL61010	61.02.02	40	21.06	693
	CL82001	82.02.24	15		
2	CL415	16.01.31	30	80.95	129
	P9704	97.01.11	30		
3	CL5293	30.02.16	–	52.02	610
	CL82003	82.02.24	12		
4	CL54002	54.01.31	80	28.07	620
	CL82006	82.02.27	15		
5	CL54003	54.02.08	90	28.05	568
	CL82004	82.02.27	8:15		
6	CL5292	43.02.22	–	37.84	525
	CL81011	81.12.25	15		
7	CL61003	61.02.12	20	35.92	541
	P9705	97.01.12	30		
8	CL5291	43.02.09	–	53.92	457
	P9706	97.01.12	30		
9	CL61002	61.02.17	30	21.02	672
	CL82002	82.02.24	–		
10	CL81012	81.12.25	15	15.05	408
	P9703	97.01.11	30		
11	CL81010	81.12.24	–	15.02	381
	P9701	97.01.02	30		
12	CL81009	81.12.24	–	15.04	335
	P9702	97.01.11	30		

Table 2.3: Precisions of proper motions for stars in different numbers of plate pairs and at different distances from the plate centre in the NGC 1817/1807 region. Units are mas yr^{-1}.

N. pairs	$r \leq 15'$				$15' < r \leq 30'$				$30' < r \leq 45'$			
	N	ϵ_{μ_x}	ϵ_{μ_y}	ϵ_μ	N	ϵ_{μ_x}	ϵ_{μ_y}	ϵ_μ	N	ϵ_{μ_x}	ϵ_{μ_y}	ϵ_μ
3—6	28	2.16	2.02	2.96	83	2.17	2.04	2.98	32	1.78	1.82	2.55
7—9	45	1.93	1.91	2.72	114	1.45	1.40	2.02	32	1.33	1.50	2.00
10 —12	146	0.89	0.86	1.24	158	0.85	0.77	1.15	23	0.94	0.98	1.36
3—12	219	1.38	1.33	1.92	355	1.44	1.37	1.99	87	1.43	1.52	2.09

$$y' = b_0 + b_1 x + b_2 y + b_3 x^2 + b_4 xy + b_5 y^2 + b_6 my \tag{2.4}$$

where m is the magnitude.

The weighted mean of the proper motion of a star obtained from every available plate pair is taken as the final value of the proper motion of the star. The proper motion weight for a star in a plate pair is determined from the epoch difference of the pair and the measuring accuracy of the stellar image.

Figure 2.1 gives the number of stars for which different numbers of plate pairs are available. More than 70% of proper motions are obtained from more than 6 plate pairs.

Table 2.3 gives the precisions of final proper motions for stars in the NGC 1817/ NGC 1807 region with different numbers of measured pairs (greater than 2) and different distances from the field centre. It is shown that, as could be expected, the precisions depend strongly on the number of plate pairs, and the greater the number of pairs, the higher the precisions of the final proper motions of the stars.

It can also be seen from Table 2.3 that there is no obvious relation between the precisions of the final proper motions and the distances of stars from the plate centre.

The mean errors of the proper motions of all 722 stars are $\epsilon_{\mu_x} = 1.42$ mas yr^{-1}, $\epsilon_{\mu_y} = 1.37$ mas yr^{-1}, and $\epsilon_\mu = 1.97$ mas yr^{-1}, where $\epsilon_\mu = \sqrt{\epsilon_{\mu_x}^2 + \epsilon_{\mu_y}^2}$. In the most precise case, the errors are found to be 1.15 mas yr^{-1} for stars with 10 to 12 plate

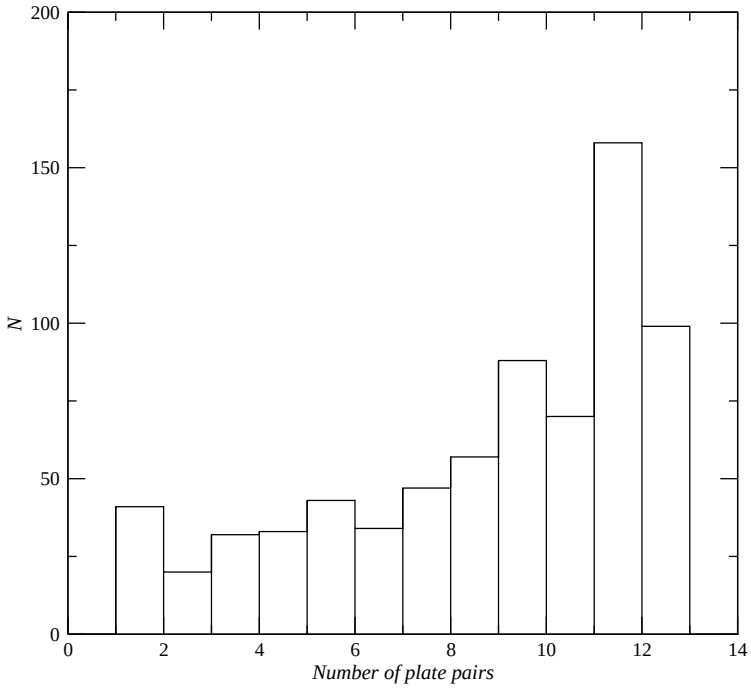

Figure 2.1: The number of stars vs the number of available plate pairs.

pairs and distances to the centre between 15' and 30'. The proper-motions error histogram can be seen in Figure 2.2, which shows the relations N versus ϵ_{μ_x}, ϵ_{μ_y} and ϵ_{μ}.

The precision of the proper motions is poorer than usual, maybe because the epoch differences of plates are not long enough or maybe due to the positioning behaviour of the PDS scanning machine.

2.3 Membership determination for two open clusters in the field: NGC 1817 and NGC 1807

The fundamental mathematical model for cluster-field segregation set up by Vasilevskis et al. (1958) and the technique based upon the maximum likelihood principle developed by Sanders (1971) have since then been continuously refined.

An improved method for membership determination of stellar clusters based on

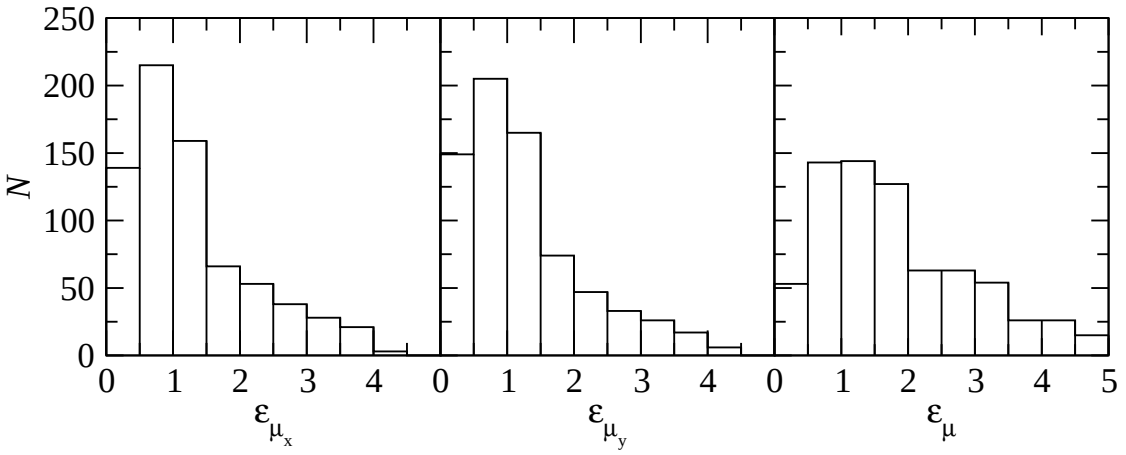

Figure 2.2: The number of stars vs the errors in proper motions (units are in mas yr^{-1}).

proper motions with different observed precisions was developed by Stetson (1980) and Zhao & He (1990). This model has been frequently used (Wang et al. 1995, 1996, 2000, Tian et al. 1996, van Leeuwen et al. 2000, among others). The spatial distribution of cluster stars and the dependence of the distribution parameters on the magnitudes of stars were considered by Su et al. (1998). Zhao et al. (1988) and Zhao & Zhao (1994) developed a statistical method on the same principle to determine the distribution parameters and membership of rich galaxy clusters. Shao & Zhao (1996) extended the above method to the situation of multiple substructures and multiple criteria, and developed a strict, rigorous, and useful mathematical model.

Tian et al. (1998) adapted this multi-substructure and multi-criterion maximum likelihood method in one-dimensional radial velocity to the case of two dimensional velocity space (relative proper motions), and determined successfully the distribution parameters and membership of a region with two open clusters. As we pointed out in the introduction, there may be two open clusters, NGC 1817 and NGC 1807, in the region examined in the present study. In order to verify this point, we will follow the same method to determine the distribution parameters and membership of the two open clusters.

The probability density function of the cluster, in the proper motion space, can be written as follows:

$$\phi_c^{\vec{v}} = \frac{1}{2\pi(\sigma_c^2+\epsilon_{\mu_{xi}}^2)^{1/2}(\sigma_c^2+\epsilon_{\mu_{yi}}^2)^{1/2}} \exp\left\{-\frac{1}{2}\left[\frac{(\mu_{xi}-\mu_{xc})^2}{\sigma_c^2+\epsilon_{\mu_{xi}}^2}+\frac{(\mu_{yi}-\mu_{yc})^2}{\sigma_c^2+\epsilon_{\mu_{yi}}^2}\right]\right\}, \quad (2.5)$$

where (μ_{xi}, μ_{yi}) are the proper motions of the i-th star, (μ_{xc}, μ_{yc}) the cluster proper motion centre, σ_c the intrinsic proper motion dispersions of the member stars and ($\epsilon_{\mu_{xi}}$,$\epsilon_{\mu_{yi}}$) are the observed errors of the proper-motion components of the i-th star.

And for the field,

$$\phi_f^{\vec{v}} = \frac{1}{2\pi(1-\rho^2)^{1/2}(\sigma_{\mu_{xf}}^2+\epsilon_{\mu_{xi}}^2)^{1/2}(\sigma_{\mu_{yf}}^2+\epsilon_{\mu_{yi}}^2)^{1/2}} \exp\left\{-\frac{1}{2(1-\rho^2)}\left[\frac{(\mu_{xi}-\mu_{xf})^2}{\sigma_{\mu_{xf}}^2+\epsilon_{\mu_{xi}}^2} - \frac{2\rho(\mu_{xi}-\mu_{xf})(\mu_{yi}-\mu_{yf})}{(\sigma_{\mu_{xf}}^2+\epsilon_{\mu_{xi}}^2)^{1/2}(\sigma_{\mu_{yf}}^2+\epsilon_{\mu_{yi}}^2)^{1/2}} + \frac{(\mu_{yi}-\mu_{yf})^2}{\sigma_{\mu_{yf}}^2+\epsilon_{\mu_{yi}}^2}\right]\right\}, \quad (2.6)$$

where (μ_{xi}, μ_{yi}) are the proper motions of the i-th star, (μ_{xf}, μ_{yf}) the field proper motion centre, ($\epsilon_{\mu_{xi}}$,$\epsilon_{\mu_{yi}}$) are the observed errors of the proper-motion components of the i-th star, $(\sigma_{\mu_{xf}}, \sigma_{\mu_{yf}})$ the field intrinsic proper motion dispersions and ρ the correlation coefficient.

On the other hand, the surface-number-density of cluster members is a function of the position. A Gaussian profile is the chosen approximation,

$$\phi_c^{\vec{r}} = \frac{1}{2\pi r_c^2}. \exp\left\{-\frac{1}{2}\left[\left(\frac{x_i-x_c}{r_c}\right)^2+\left(\frac{y_i-y_c}{r_c}\right)^2\right]\right\}, \quad (2.7)$$

where (x_c,y_c) is the centre of the cluster, and r_c the characteristic radius.

And a uniform distribution of field stars is adopted,

Table 2.4: Distribution parameters and their uncertainties for NGC 1817 and NGC 1807. The coordinates are given in J2000, epoch 1991.25. The units of μ and σ are in mas yr^{-1}.

	N. stars	α_{J2000} (5^h+)	δ_{J2000} ($16^\circ+$)	r_c	μ_x	μ_y	σ_c	σ_{μ_x}	σ_{μ_y}	ρ
NGC 1817	440	$12^m20^s.14$	$43'47".45$	$13'.91$	2.33	5.20	3.45			
		$\pm2^s.3$	$\pm32"$	$\pm0'.55$	±0.22	±0.21	±0.10			
NGC 1807	27	$10^m55^s.66$	$23'23".39$	$5'.14$	-1.82	5.30	2.39			
	±4	$\pm4^s.8$	$\pm48"$	$\pm0'.65$	±0.68	±0.76	±0.37			
field	250				-5.30	-1.28		15.0	14.1	-0.045

$$\phi_f^{\vec{r}} = \frac{1}{\pi r_{\max}^2} \tag{2.8}$$

where $r_{\max}$ is the radius of the considered area.

The distribution of all stars in the region can, then, be described as follows:

$$\Phi = \Phi_c + \Phi_f = \sum_{c=1}^{2} n_c \cdot \phi_c^{\vec{v}} \cdot \phi_c^{\vec{r}} + n_f \cdot \phi_f^{\vec{v}} \cdot \phi_f^{\vec{r}}. \tag{2.9}$$

respectively, $\phi_c^{\vec{r}}$, $\phi_f^{\vec{r}}$, $\phi_c^{\vec{v}}$, and $\phi_f^{\vec{v}}$, are the normalised distribution functions of cluster members and field stars in the position ($\vec{r}$) and relative proper motion ($\vec{v}$) spaces. With n_c, the number of cluster stars, and n_f, the number of field stars.

2.3.1 Results and discussion

The unknown parameters for this distribution are $(n_c, x_c, y_c, r_c, \mu_{xc}, \mu_{yc}, \sigma_c)_{c=1,2}$ and $(n_f, \mu_{xf}, \mu_{yf}, \sigma_{\mu_x f}, \sigma_{\mu_y f}, \rho)$. Membership probabilities of the i-th star belonging to the c-th cluster can be calculated from the following,

$$P_c(i) = \frac{\Phi_c(i)}{\Phi(i)} \qquad (c = 1, 2). \tag{2.10}$$

According to the standard maximum likelihood method we obtained the distribution parameters and their corresponding uncertainties given in Table 2.4.

Table 2.5: The cross-identification of stars in Table 2.6 with the TYCHO and PPM Catalogues.

Table 2.6	TYCHO	PPM	Table 2.6	TYCHO	PPM	Table 2.6	TYCHO	PPM
48	1283 0618		59	1283 1012		97	1287 1643	
101	1287 1461		110	1287 1849		137	1283 0972	
140	1283 0967		207	1287 1276	120726	215	1287 1736	
244	1283 0546		262	1283 0850		290	1283 0927	120723
297	1283 0843	120713	298	1283 0827		315	1283 0675	120714
402	1283 1299		473	1283 0586		476	1283 0608	
527	1283 0699		530	1283 0779	120705	547	1283 1086	120700
561	1283 0896	120703	572	1282 0353	120694	576	1282 0348	
653	1287 1837		683	1282 0399		703	1282 0600	120687
709	1282 0398	120684	731	1282 0318		767	1286 0220	120682
797	1282 0534		807	1282 0452	120680	813	1282 0504	
819	1282 0501		822	1282 0550	120673	825	1282 0569	120672
827	1282 0576		831	1282 0689		835	1282 0586	120674
881	1282 0253							

Equatorial coordinates were computed using the Tycho Catalogue (ESA 1997) as reference stars. Forty stars from this catalogue are in the region under study. Following Galadí-Enríquez et al. (1998b), the best fitting of these reference stars was a second order pair of equations. The cross-identifications of these 40 stars are given in Table 2.5. Only 15 stars were found in this region from the PPM Catalogue (Röser & Bastian 1991), and their identification is also included in the same table.

Table 2.6[3] lists the results for all 722 stars in the region of the two open clusters: column 1 is the ordinal star number; columns 2 and 3 are α_{J2000} and δ_{J2000} with epoch 1991.25; columns 4 and 5 are the proper motions; colums 6 and 7 are the standard errors of the proper motions; columns 8, 9, and 10 are probabilities of stars belonging to NGC 1817 (P_1), NGC 1807 (P_2), and the field (P_f) respectively; and column 11 is the number of plate pairs used.

Figures 2.3 and 2.4 show the proper motion vector-point diagram and the distribution on the sky for all the measured stars respectively, where " $\circ$ " denotes a star with $P_1 \geq 0.7$ of being member of NGC 1817, " $\bullet$ " a star with $P_2 \geq 0.7$ of being member of NGC 1807, and all other stars are considered field stars indicated by "+". It can be noted from the two figures that the centres in positional space

[3]Table 2.6 is only available in electronic form at the CDS via anonymous ftp to cdsarc.u-strasbg.fr (130.79.128.5) or via `http://cdsweb.u-strasbg.fr/cgi-bin/qcat?J/A+AS/133/387/`

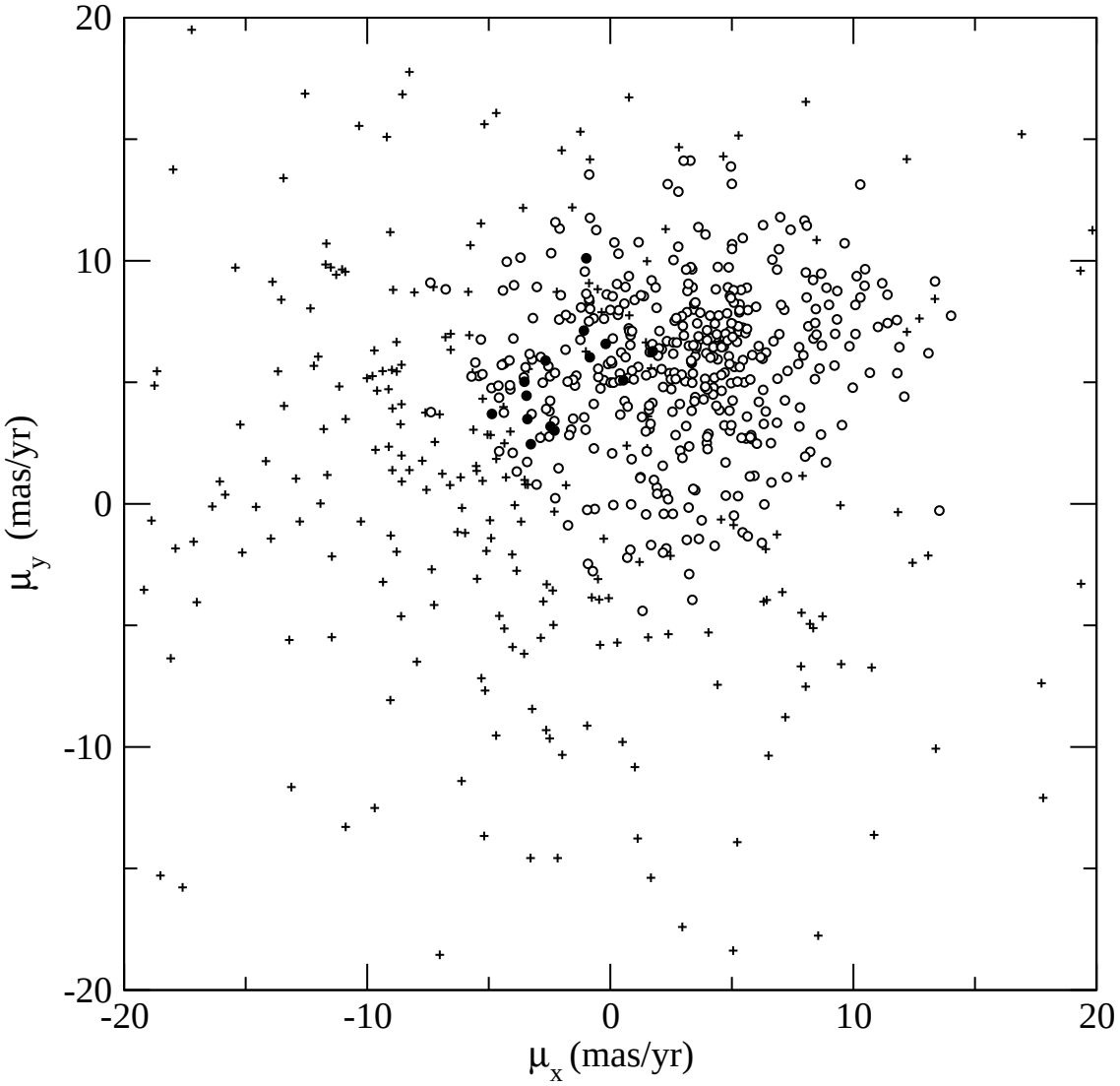

Figure 2.3: The proper motion vector-point diagram of NGC 1817 and NGC 1807. ("○" denotes a star with $P_1 \geq 0.7$ of being member of NGC 1817, '•" a star with $P_2 \geq 0.7$ of being member of NGC 1807, "+" a field star.)

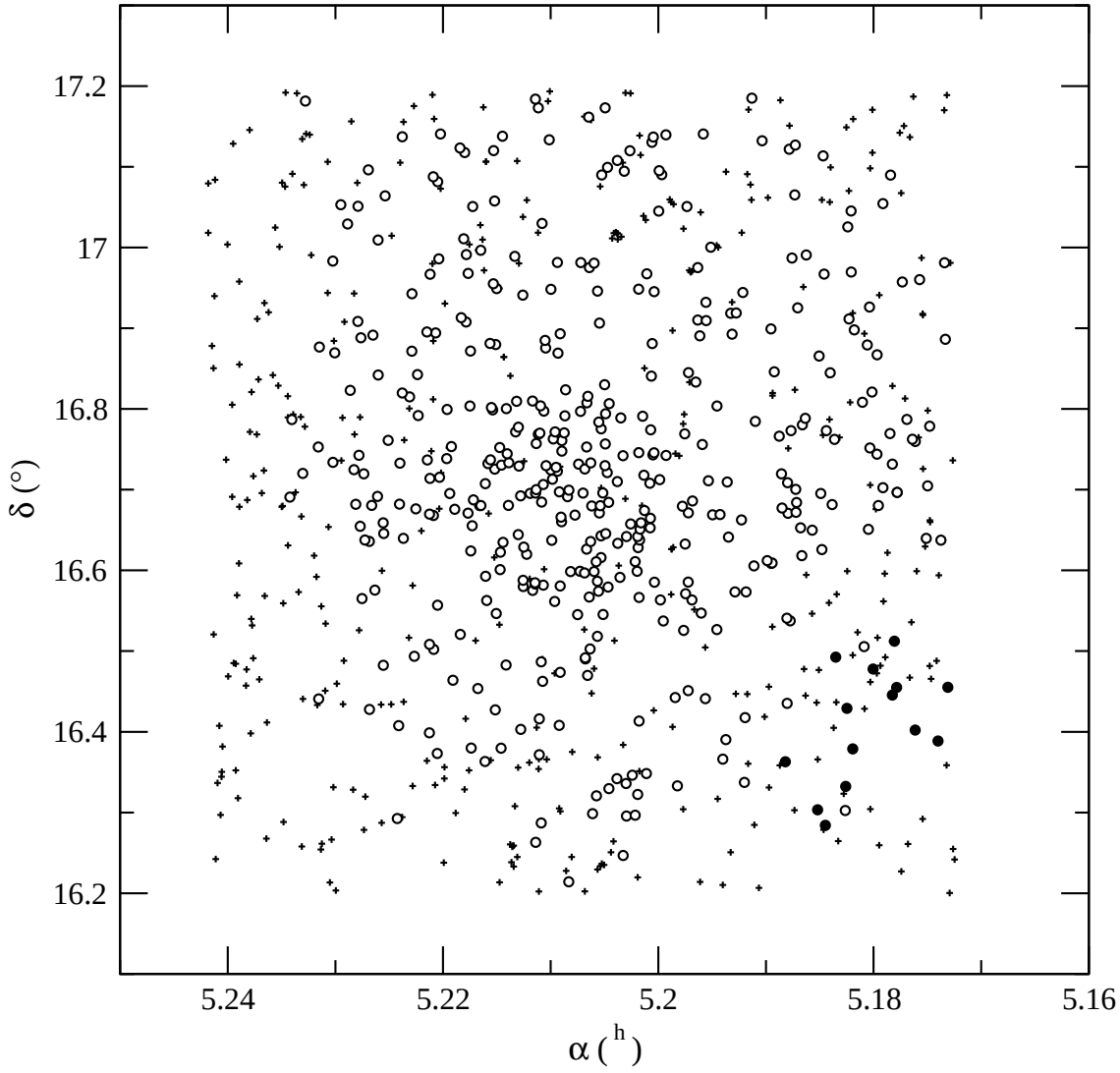

Figure 2.4: The position distribution of stars in NGC 1817 and NGC 1807 area. ("○" denotes a star with $P_1 \geq 0.7$ of being member of NGC 1817, "•" a star with $P_2 \geq 0.7$ of being member of NGC 1807, "+" a field star.)

are clearly separated while the centres in velocity (proper motion) space for the two open clusters not so clearly. From the distribution parameters listed in Table 2.4 we can observe that the dispersion of the cluster proper motions is somewhat too big. In principle, this could be due to two reasons: the intrinsic velocity dispersion of the cluster members on one hand, and the precision of the proper motions on the other hand. The dispersion of proper motions compared to the mean internal errors seems to indicate that the velocity dispersion of members is larger than in other clusters, if the distance of 1800 pc (Harris & Harris 1977) is assumed.

The angular diameter of NGC 1817 presented here is significantly larger than the values found by previous authors. Cuffey (1938) gave an estimation of $15'$ for the angular diameter based on his photometric study of the central region. We found a larger diameter based on a complete astrometric study of all the region. NGC 1817 has an halo more extended that can be recognised in a visual inspeccion of the area. Further studies using photometric data (Chapter 3) and radial velocities (Section 2.6.4), will be very helpful on this subject.

The membership probability histogram (Figure 2.5) shows a clear separation between the stars classified as cluster members and those considered field stars. We find that the number of stars with membership probabilities higher than 0.7 for NGC 1817 and NGC 1807 are 416 and 14 respectively, and their average membership probabilities are 0.93 and 0.83 respectively, i.e., contamination by field stars is expected to be only 7% and 17% for the two clusters.

Till this point, all of our work indicates that the determination of two open clusters is successful: NGC 1817 and NGC 1807. But, unfortunately, the fact that NGC 1807 cluster has such a small number of stars added to a large intrinsic dispersion, makes the reliability of the results questionable. Conclusive results for this cluster will come from photometry (see Chapter 3) and radial velocities studies (see Section 2.6.4).

2.3.1.1 Effectiveness of membership determination

Contamination by background and foreground objects through the influence of the observational projection effect cannot be avoided. Following Shao & Zhao (1996), we can judge quantitatively how effective the results of our membership determination was. The effectiveness of membership determination is set as:

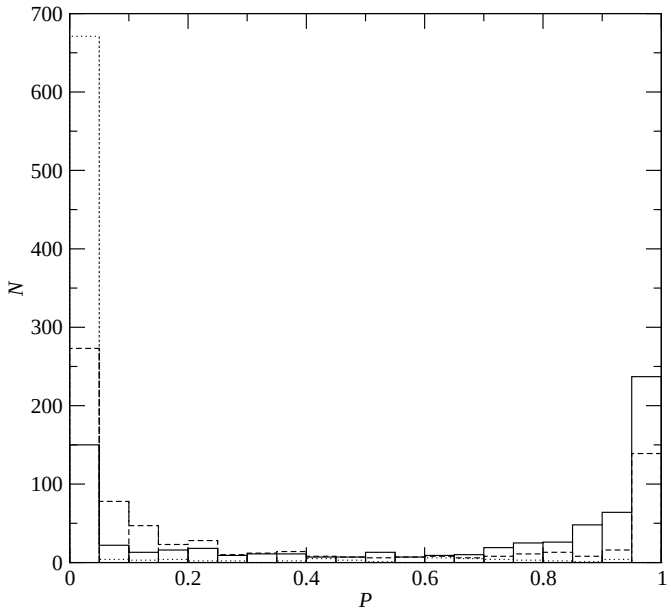

Figure 2.5: The histogram of membership probability of NGC 1817 (solid line), NGC 1807 (dotted line) and field stars (dashed line)

$$E = 1 - \frac{N \sum_{i=1}^{N} \{P(i)\,[1 - P(i)]\}}{\sum_{i=1}^{N} P(i) \sum_{i=1}^{N} [1 - P(i)]} \tag{2.11}$$

where the larger E is, the more effective the membership determination is.

So we can determine that the effectiveness of membership determination is 0.68 and 0.63 for NGC 1817 and NGC 1807, respectively. It is shown in Figure 3 of Shao & Zhao (1996) that the effectiveness of membership determination of 43 open clusters range from 0.20 to 0.90 and the peak value is 0.55. Compared with previous works (Shao & Zhao 1996; Tian et al. 1998), we can see that the effectiveness of membership determination for the two open clusters is significantly high in both cases.

However, it must be stated that this quantity, E, traditionally named "effectiveness" in the literature, could be regarded more precisely as a *contrast* function. This function is a measure of the relative importance of the cluster(s) frequency function(s) compared to the underlying field frequency function. Thus, it is not related to the quality of the calculations that have been done, nor it is any physical property of the cluster(s). The same cluster observed with the same instruments

against a richer background would yield a lower E. Also, it is worth noting that the effectiveness is computed from the fit functions and, as a consequence, if the mathematical model used to describe the data would result inadequate, the effectiveness linked to the fit functions would not have much meaning. On the opposite side, a well modelised set of frequency functions would yield an E value indicative of the extent of field contamination if cluster membership was assigned on the only basis of the probabilities derived from these data.

2.4 Motivation for a new astrometric analysis

Aiming to physically characterise the cluster or clusters present in the area, we undertook a wide field photometric study (1998-2000) of a $65' \times 40'$ area around NGC 1817/NGC 1807 in the $uvby - H_\beta$ system down to a limiting magnitude $V \sim 22$. This work (described in length in Chapter 3) confirm that NGC 1807 is not a real physical open cluster and that only one very extended open cluster, NGC 1817, covers the area (see Section 3.5).

Moreover, Mermilliod et al. (2003) have determined radial velocities of red giant stars in the area and their results point, too, towards the non-existence of NGC 1807 as a real physical cluster. The stars in the region assigned to NGC 1807 have discordant radial velocities and two of them have radial velocities compatible with those of NGC 1817 (see Sections 2.6.4 and 3.4).

The inappropriate assumption of there being two open clusters in the membership analysis of Section 2.3, could affect the conclusions, as will be shown later. For this reason, a new membership determination seems advisable and two completely different methods have been used for this purpose. This has never been done before on the same set of data, which makes our comparison specially interesting.

Once decided to re-compute the member segregation, we preferred to re-elaborate the original material to introduce some improvements in the proper-motion calculation. After obtaining the photometric analysis results, the release of the Tycho-2 Catalogue allows an accurate transformation from x and y coordinates derived from plate measurements to the ICRS system, leading to proper motions computed directly in absolute sky coordinates, which would make the resulting catalogue much more useful for further studies. Finally, as is shown below, a central overlap tech-

nique applied to the PDS scan data of all the available 25 plates, one more than in Section 2.2 (plate CL82005), makes it possible to enlarge the sample studied by about one hundred stars.

A previous determination of mean proper motions of open clusters by Dias et al. (2002b) based on the Tycho-2 Catalogue (Høg et al. 2000) gives absolute values for NGC 1817. But the study is based on only 19 stars in an area of 15′, with ten stars considered as cluster members.

2.5 Absolute proper motions: Central overlap technique

In this section we determine precise absolute proper motions of 810 stars within a $1\overset{\circ}{.}5 \times 1\overset{\circ}{.}5$ area in the NGC 1817/NGC 1807 region, from automatic PDS measurements of 25 plates. The estimated membership probabilities taking into account only one extended cluster led us to an improved complete astrometric study of the cluster area.

At the time of the first reduction only 15 PPM (Röser & Bastian 1991) stars were available as standard stars. So the reduction of relative proper motions based on plate pairs was the appropiate choice. Here, the absolute proper motions in the region of NGC 1817 were obtained by following the central overlap procedure (Russel 1976; Wang et al. 1995, 1996, 2000).

The central overlap method simultaneously determines the plate-to-plate transformation parameters, the star motions and their errors. This method has rigorous mathematical foundations (Eichhorn 1988), but its computational requirements are so huge that, in practice, it cannot be implemented in its strict formulation. The usual approach to the method is generally known as iterative central-overlap algorithm, and implies the separation of the determination of plate and star parameters in consecutive steps that are iterated until convergence is achieved. This procedure is known to be equivalent, in practice, to the one-step block-adjustment approach, and has been extensively used during the last decades (Wu et al. 2002, Galadí-Enríquez et al. 1998b among others). In applying the central overlap technique, the plate measurements are first reduced to a reference catalogue system, using the

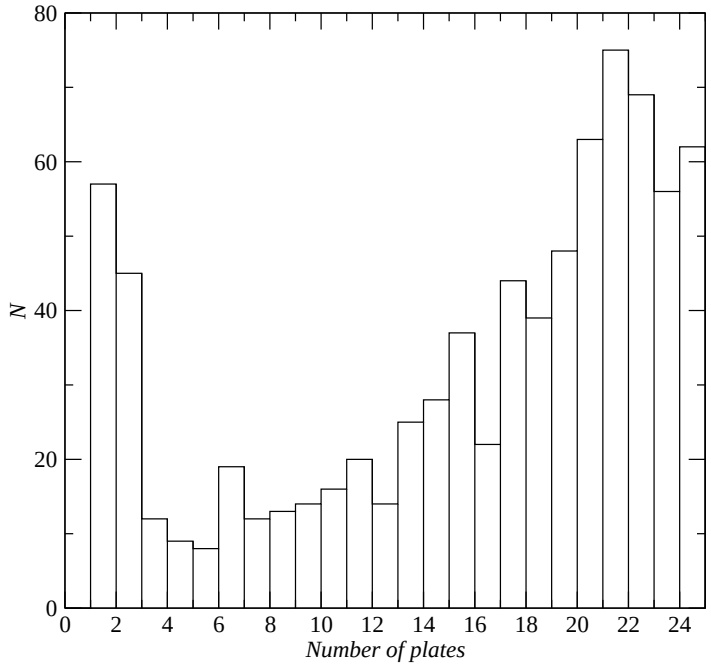

Figure 2.6: The number of stars (N) vs the number of available plates

data for those stars with reference positions to determine the plate constants. As initial catalogue, 86 stars from the Tycho-2 Catalogue at epoch J2000 (Høg et al. 2000) were selected. The plate constants are then applied to all the stellar measurements, giving equatorial coordinates for each star from each plate on which the star appears. The data for each star are then selected and solved by least squares for improved positions and proper motions. These revised star parameters form a new catalogue, which is on the system of the original reference catalogue, but has been strengthened and expanded to include additional stars. This new catalogue is used for a new determination of the plate constants, and the resulting positions solved for a further improvement of the stars positions and proper motions.

The iteration requires equatorial coordinates for each star on each plate as starting values. After positions for each star on each plate are computed, proper motions are determined from a linear regression of position versus time. If the error of one proper motion component exceeded 3σ, the most deviant measurement was discarded and the proper motion recomputed, until the error fell bellow the mentioned limit. In the next iteration, all stars with precise proper motions are used as reference stars for a new transformation from plate to spherical coordinates. In the

first iteration, only linear terms were used; in the second iteration, higher order terms were included. Only significant transformation terms were kept. To select the best plate constant model, we used Eichhorn & Williams' criterion (Eichhorn & Williams 1963, Wang et al. 1982) and evaluated nine different geometric models and four possible terms related with magnitude (linear, quadratic and distorsion) and coma. The result was a model with six linear constants on coordinates, a magnitude and a coma term, and a magnitude distortion term:

$$x' = a_0 + a_1 x + a_2 y + a_3 m + a_4 m x + a_5 m x (x^2 + y^2) \tag{2.12}$$

$$y' = b_0 + b_1 x + b_2 y + b_3 m + b_4 m y + b_5 m y (x^2 + y^2) \tag{2.13}$$

We require that any star remaining in the final catalogue has at least one measurement from the modern epoch plates.

The whole process is iterated until convergence is achieved. The criteria for convergence were: mean differences in position smaller than 1.1 mas, r.m.s. smaller than 3.6 mas and differences in proper motion below 0.1 mas yr^{-1}. The final outcome results in 810 stars.

Table 2.7 shows the mean precisions of final proper motions for stars in the NGC 1817 region detected on more than 3 plates. 21 stars with errors greater than 3 mas yr^{-1} were not included. Errors for stars on only two plates were not computed. The precision of the final proper motions strongly depends on the number of plates. Figure 2.6 gives the number of stars for which various numbers of plates are available. More than 85% of proper motions were obtained from at least 5 plates.

Thanks to the addition of one more plate and the use of the overlap technique we determined proper motions for 88 stars more than in Section 2.2. Most of these recovered stars were measured in 2-3 plates. In addition, the mean number of plates per star also increased by a factor 1.8 (up to eight more plates). The errors are a factor of 0.77 better than in Section 2.2. Figure 2.7 shows the errors in the proper motions compared to those in Section 2.2.

The mean errors in the proper motions for more than 80% of the stars are $\epsilon_{\mu_\alpha \cos\delta} = 1.16$ mas yr^{-1}, $\epsilon_{\mu_\delta} = 0.96$ mas yr^{-1} and $\epsilon_\mu = 1.55$ mas yr^{-1}, where $\epsilon_\mu = \sqrt{\epsilon^2_{\mu_\alpha \cos\delta} + \epsilon^2_{\mu_\delta}}$. In the most precise case, the errors are 0.97 mas yr^{-1} for stars with more than 21 plates (32% of stars). Figure 2.8 shows the distribution of proper motion errors with the number of stars: N vs $\epsilon_{\mu_\alpha \cos\delta}$, ϵ_{μ_δ} and ϵ_μ.

Table 2.7: Mean precisions of proper motions as a function of the number of plates in the NGC 1817 region. (Units are mas yr^{-1}.) Columns "N. plates" and "N" give the number of plates and stars, respectively.

N. plates	N	$\epsilon_{\mu_\alpha \cos\delta}$	ϵ_{μ_δ}	ϵ_μ
3	12	0.986	1.037	1.590
4	10	1.359	1.235	1.932
5	7	1.593	1.455	2.279
6	7	1.624	1.338	2.249
7	14	1.790	1.520	2.403
8	10	1.996	1.390	2.464
9	12	1.720	1.765	2.529
10	13	1.684	1.429	2.249
11	13	2.012	1.658	2.655
12	20	1.782	1.420	2.351
13	14	1.611	1.290	2.136
14	24	1.635	1.299	2.134
15	28	1.515	1.486	2.166
16	37	1.531	1.095	1.933
17	21	1.514	1.206	1.982
18	44	1.172	1.023	1.591
19	38	1.228	0.950	1.592
20	48	1.242	1.056	1.667
21	63	1.076	0.829	1.400
22	75	0.842	0.720	1.131
23	69	0.940	0.677	1.179
24	56	0.630	0.559	0.853
25	62	0.471	0.429	0.646
> 3	685	1.162	0.958	1.545

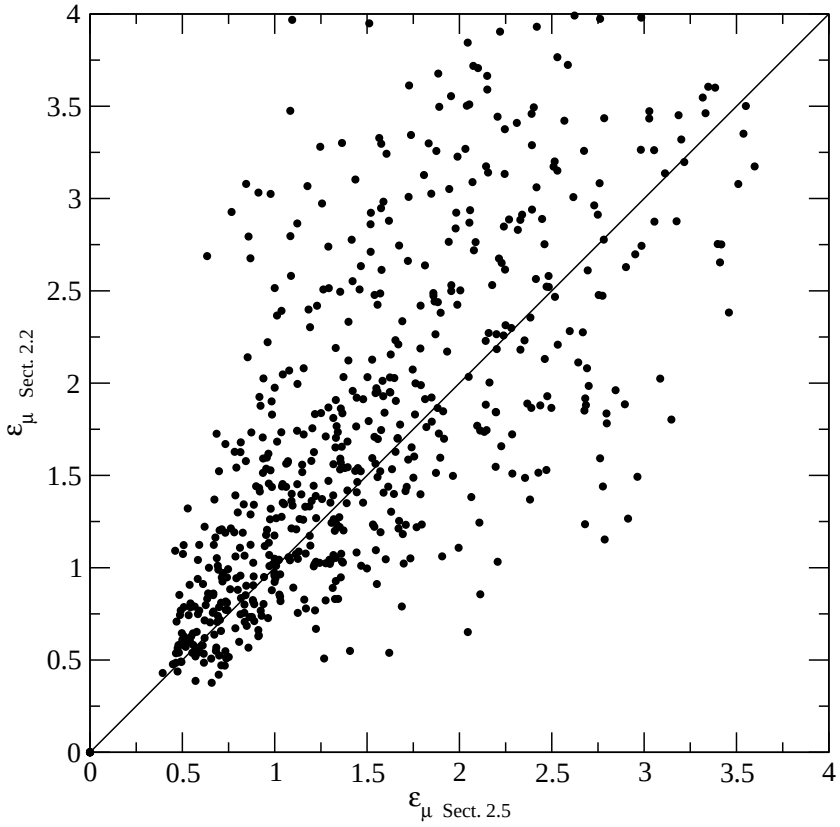

Figure 2.7: Proper motion errors vs those in Section 2.2.

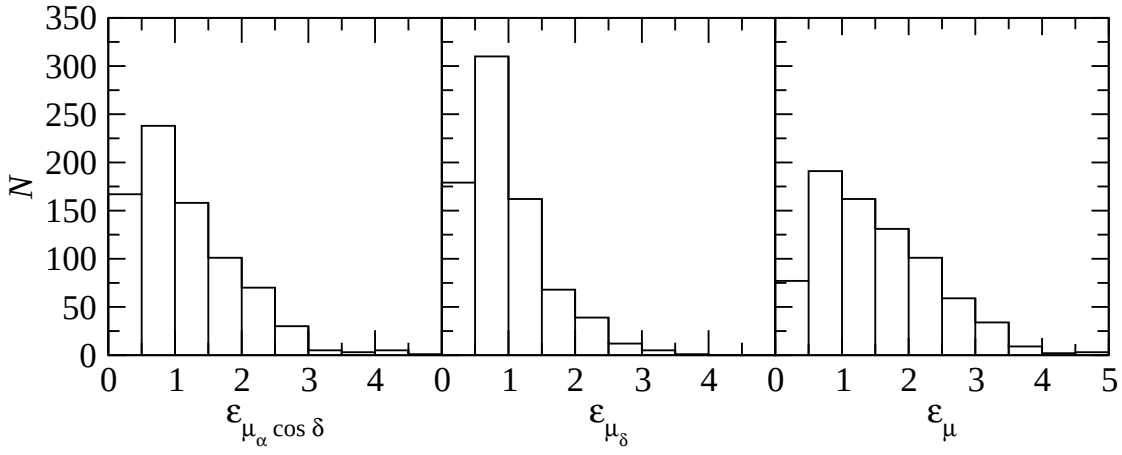

Figure 2.8: The number of stars vs the errors in proper motions (units are in mas yr^{-1})

Figure 2.9 gives $\mu_\alpha \cos\delta$, μ_δ and their errors as a function of V magnitude of the stars in common with Chapter 3. Since the CCD photometry in Chapter 3 covers a smaller area than the astrometric catalogue from this chapter, these graphs cannot display the data for all the stars present in this study, but they describe well the behaviour of the data as a function of apparent brightness. No systematic trends in proper motion are apparent as a function of magnitude for member stars (see Section 2.6.4).

Our absolute proper motions and their errors are compared with those of the Tycho-2 Catalogue in Figure 2.10. Mean differences in the sense ours minus Tycho-2 are -0.099 ($\sigma = 2.592$) and 0.659 ($\sigma = 2.557$) mas yr^{-1} in $\mu_\alpha \cos\delta$ and μ_δ, respectively. A linear fit to the proper motion data gives us:

$$\mu_\alpha \cos\delta = -0.010\ (\pm 0.300) + 0.988\ (\pm 0.014) \cdot (\mu_\alpha \cos\delta)_{\mathrm{Tyc2}}\ ;\ r = 0.992$$

$$\mu_\delta = 0.406\ (\pm 0.288) + 0.974\ (\pm 0.010) \cdot (\mu_\delta)_{\mathrm{Tyc2}}\ ;\ r = 0.995$$

where r is the correlation coefficient.

2.6 Membership determination for only one cluster in the field: NGC 1817

From the absolute proper motions obtained we can now calculate the membership probabilities of having only one cluster in the field. As already mentioned in Section 2.5 we will apply two completely different methods for this purpose: the classical parametric way and the non-parametric one. Being a very extended cluster with low spatial contrast from the field, we decided this time not to impose a spatial distribution in the parametric, classical way. In the non-parametric method, the spatial information will be studied separately from the kinematical information and then we will decide about its usefulness.

2.6.1 The classical approach

After many trials, we chose to use the maximum likelihood method with a 9-parametric Gaussian model for the frequency function in the kinematical plane only,

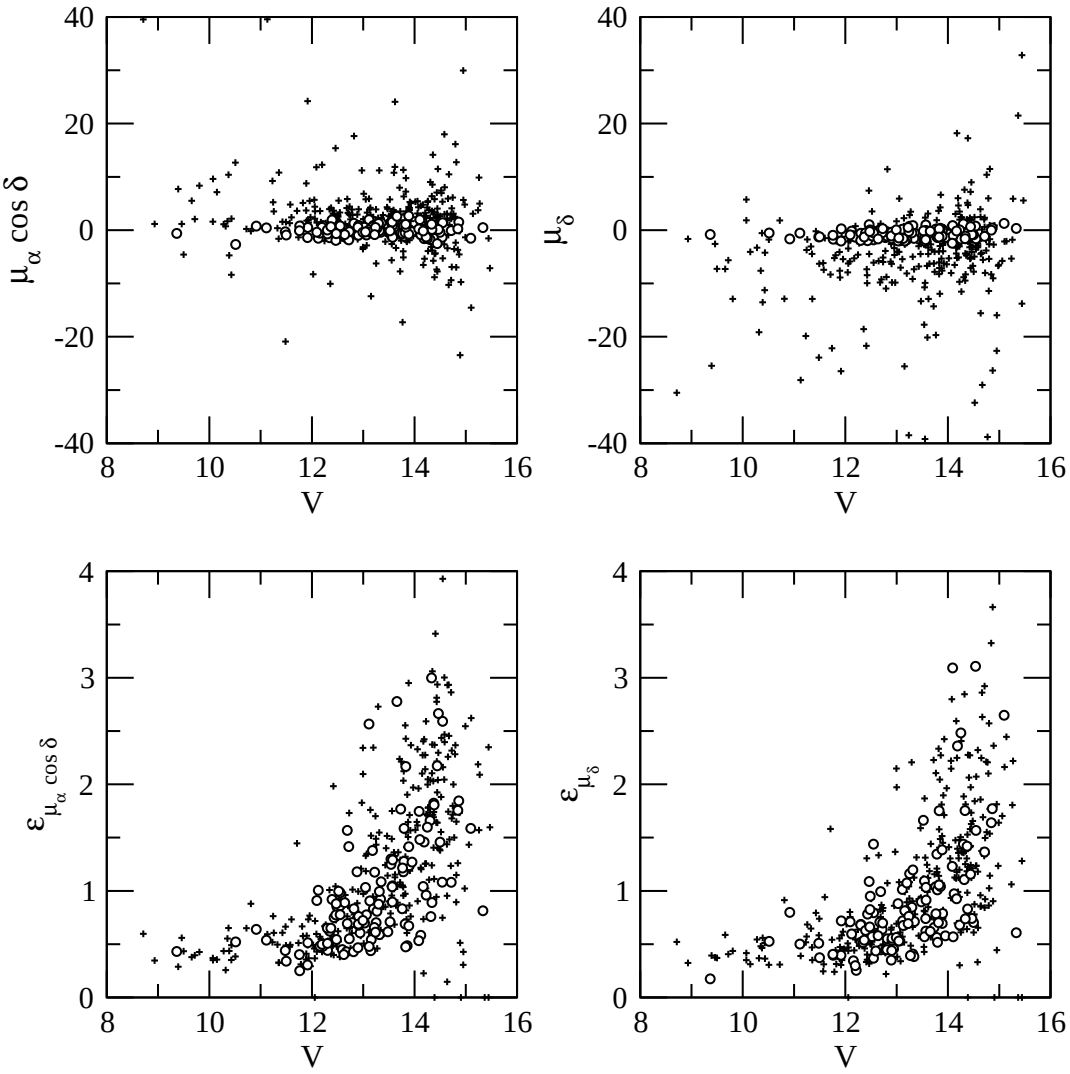

Figure 2.9: Proper motions (top) and their errors (bottom) vs V apparent magnitude, for the stars in common with the photometric study (Chapter 3). Open circles denote selected member stars (Section 2.6.4). Null errors are from proper motions calculated with only two plates, (units are mas yr^{-1}).

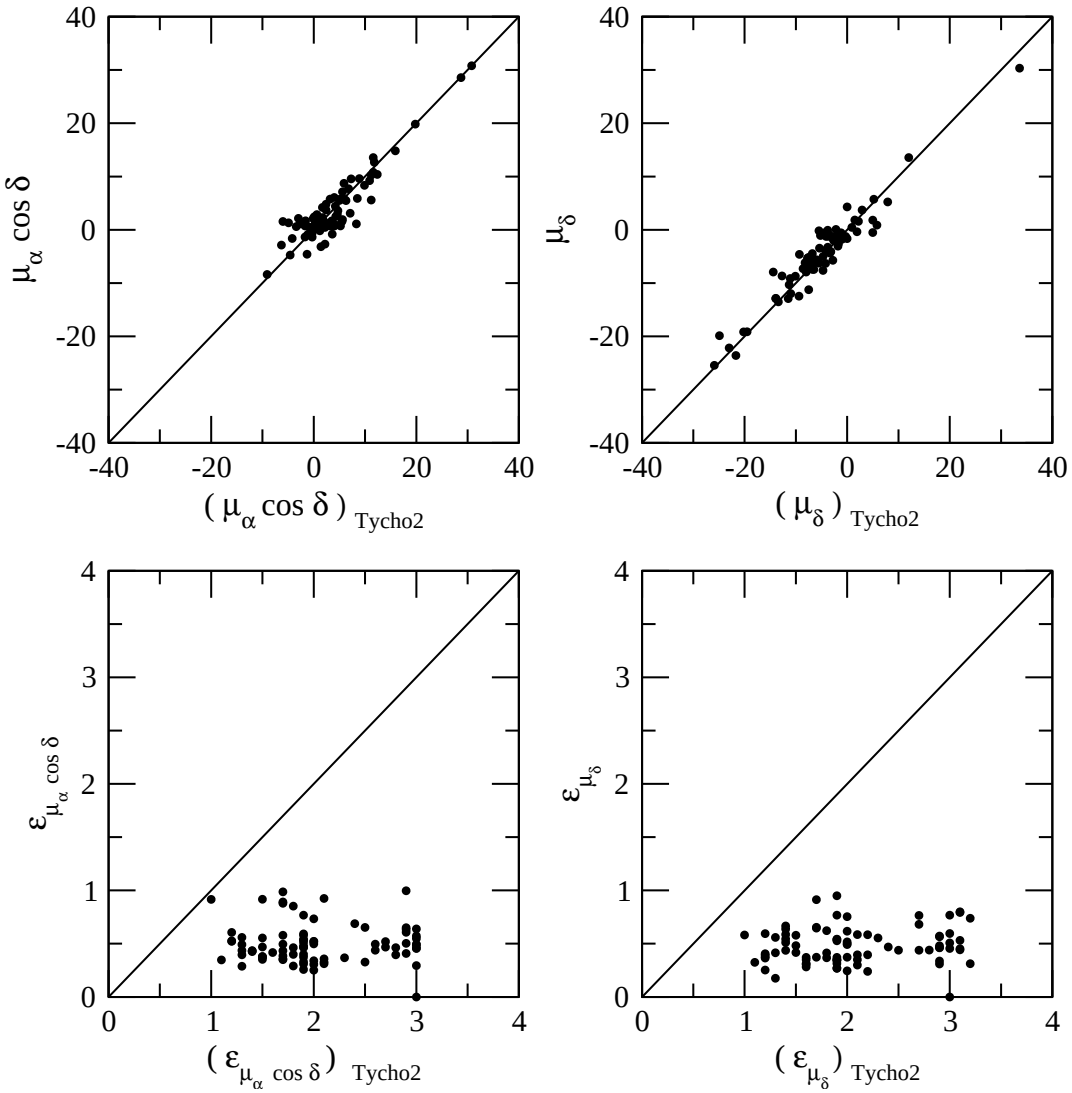

Figure 2.10: Proper motions and their errors from this study compared to those in Tycho-2 Catalogue (units are mas yr^{-1}).

as follows:

$$\Phi \ = \Phi_c + \Phi_f = n_c \cdot \phi_c + n_f \cdot \phi_f, \tag{2.14}$$

where ϕ_c, and ϕ_f, are the probability density functions of cluster members and field stars, respectively, in the proper motion space, with n_c the normalised number of cluster stars, and n_f the normalised number of field stars.

The probability density function for the i-th star of the cluster can be written now for absolute proper motions as follows:

$$\begin{aligned}\phi_c(i) \ = \ & \frac{1}{2\pi(\sigma_c^2+\epsilon^2_{(\mu_\alpha\cos\delta)_i})^{1/2}(\sigma_c^2+\epsilon^2_{(\mu_\delta)_i})^{1/2}} \\ & \exp\left\{-\frac{1}{2}\left[\frac{[(\mu_\alpha\cos\delta)_i-(\mu_\alpha\cos\delta)_c]^2}{\sigma_c^2+\epsilon^2_{(\mu_\alpha\cos\delta)_i}}+\frac{[(\mu_\delta)_i-(\mu_\delta)_c]^2}{\sigma_c^2+\epsilon^2_{(\mu_\delta)_i}}\right]\right\},\end{aligned} \tag{2.15}$$

where $[(\mu_\alpha\cos\delta)_i\ ,(\mu_\delta)_i]$ are the proper motions of the i-th star, $[(\mu_\alpha\cos\delta)_c,(\mu_\delta)_c]$ the cluster mean proper motion, σ_c the intrinsic proper motion dispersions of member stars and $[\epsilon_{(\mu_\alpha\cos\delta)_i},\epsilon_{(\mu_\delta)_i}]$ the observed errors on the proper motion components of the i-th star.

Analogously, for the field we have:

$$\begin{aligned}\phi_f(i) = \ & \frac{1}{2\pi(1-\rho^2)^{1/2}(\sigma^2_{(\mu_\alpha\cos\delta)_f}+\epsilon^2_{(\mu_\alpha\cos\delta)_i})^{1/2}(\sigma^2_{(\mu_\delta)_f}+\epsilon^2_{(\mu_\delta)_i})^{1/2}} \\ & \exp\left\{-\frac{1}{2(1-\rho^2)}\left[\frac{[(\mu_\alpha\cos\delta)_i-(\mu_\alpha\cos\delta)_f]^2}{\sigma^2_{(\mu_\alpha\cos\delta)_f}+\epsilon^2_{(\mu_\alpha\cos\delta)_i}}\right.\right. \\ & \left.\left.-\frac{2\rho[(\mu_\alpha\cos\delta)_i-(\mu_\alpha\cos\delta)_f][(\mu_\delta)_i-(\mu_\delta)_f]}{[\sigma^2_{(\mu_\alpha\cos\delta)_f}+\epsilon^2_{(\mu_\alpha\cos\delta)_i}]^{1/2}[\sigma^2_{(\mu_\delta)_f}+\epsilon^2_{(\mu_\delta)_i}]^{1/2}}+\frac{[(\mu_\delta)_i-(\mu_\delta)_f]^2}{\sigma^2_{(\mu_\delta)_f}+\epsilon^2_{(\mu_\delta)_i}}\right]\right\},\end{aligned} \tag{2.16}$$

where $[(\mu_\alpha\cos\delta)_f,(\mu_\delta)_f]$ are the field mean proper motion, $[\sigma_{(\mu_\alpha\cos\delta)_f},\sigma_{(\mu_\delta)_f}]$ the field intrinsic proper motion dispersions and ρ is the correlation coefficient.

The unknown parameters for the assumed Φ distribution are $[n_c,\ (\mu_\alpha\cos\delta)_c,\ (\mu_\delta)_c,\ \sigma_c]$ for the cluster and $[(\mu_\alpha\cos\delta)_f,\ (\mu_\delta)_f,\ \sigma_{(\mu_\alpha\cos\delta)_f},\ \sigma_{(\mu_\delta)_f},\ \rho]$ for the field

population. Membership probability of the i-th star belonging to the cluster can be calculated from $P_c(i) = \Phi_c(i)/\Phi(i)$ as in Equation (2.10) now for only one cluster.

The quality of the fit should be optimised near the vector point diagram (VPD) region occupied by the cluster stars, where the model is most crucial for providing reliable membership determinations. Outliers cause the estimated distribution of field stars to be flatter than the actual one, thus increasing the final probability of cluster membership (Kozhurina-Platais et al. 1995, Cabrera-Caño & Alfaro 1985, Zhao & Tian 1985a, Zhao et al. 1982). To minimise the effect of high proper-motion field stars in the model, we restricted the membership determination to the range $|\mu| < 30$ mas yr^{-1}.

By applying the standard maximum likelihood method, several drawbacks of the parametric method were identified. The cluster motion is not very well separated from the mean field motion, making the convergence of the results unstable and producing an unrealistic intrinsic velocity dispersion of the cluster (as suggested in Section 2.3.1): the circular Gaussian distribution intended to fit the cluster tends to assume an excessive width to improve the representation of the field distribution. This does not happen when this method is applied to dense clusters that stand out on the field, when the field population represents a small fraction of the total number of stars. But this behaviour seems unavoidable in situations like ours, with a cluster with low contrast with the field. In these cases, the parametrisation of the field model is difficult and, at the same time, crucial, because the residuals of an inaccurate field model can be of the same order of or bigger than the cluster signal, and the membership calculations can be affected by this. As the cluster is at a distance of about 1.8 kpc, it is clear that our measurements lack the resolution needed to resolve its internal velocity dispersion. And thus, to be on the safe side we decided to set the cluster intrinsic dispersion to zero in order to minimise the problem just outlined. This way, the model will assign to the cluster Gaussian distribution a width related only to the measurement errors. We have tried fixing different internal velocity dispersions for the cluster, in the range of plausible velocities (1 to 3 km s^{-1}) and distances (1.5 to 2 kpc), but the slight differences do not affect the values obtained or the segregation. By applying the standard maximum likelihood method, we obtained the 9 distribution parameters and their corresponding uncertainties shown in Table 2.8.

Table 2.8: Distribution parameters and their uncertainties for the NGC 1817 cluster and the field. The units of μ and σ are mas yr^{-1}

	n_c	$\mu_\alpha \cos\delta$	μ_δ	$\sigma_{\mu_\alpha \cos\delta}$	σ_{μ_δ}	ρ
NGC 1817*	0.261	0.29	−0.96			
	±0.020	±0.10	±0.07			
field		2.29	−4.25	5.69	6.38	−0.08
		±0.02	±0.27	±0.02	±0.14	±0.03

* $\sigma_c = 0$ (fixed)

2.6.1.1 Effectiveness of membership determination

As explained in Section 2.3.1.1 and following Equation (2.11) we can calculate the effectiveness of membership determination with this new approach (only one cluster in the area). We find a value of $E = 0.67$ for NGC 1817, being slightly lower but similar to the value found in Section 2.3.

Taking into account that in this new approach we have not used any spatial information, this lower value can be more readily understood. The fact of not imposing any spatial shape to the cluster should free the membership of every star independently of its location. For low contrast clusters, spatial information will increase the value of E, artificially amplifying the contrast between cluster and field frequency functions.

2.6.2 The non-parametric approach

As discussed by many authors (Cabrera-Caño & Alfaro 1990, for example), the membership determination based on fits of parametric probability density functions (PDFs) has several limitations. A circular bivariate function is a good representation of the cluster PDF if the intrinsic velocity dispersion of the cluster is not resolved, or if it is resolved but symmetric. Moreover, the choice of an elliptic bivariate Gaussian function for the field distribution is known to be unrealistic. The proper motion distribution of field stars has an intricate structure dominated by the combination of

solar motion and Galactic differential rotation. Furthermore, real field distribution wings are stronger than those predicted by a Gaussian model (Marschall & Van Altena 1987). Soubiran (1992) modeled the field population in the direction of the North Galactic Pole by means of the sum of three Gaussian distributions. But adding further Gaussians to the field in the classical parametric model has been shown to give poor results (Galadí-Enríquez et al. 1998a) in some cases.

In our case, as seen in Sections 2.3 and 2.6.1, the cluster mean proper motion is close to the maximum of the field distribution and the cluster is loosely concentrated, making necessary an accurate model of the field distribution. Following Galadí-Enríquez et al. (1998a), we perform an empirical determination of the PDFs without relying on any previous assumption about their profiles. For a sample of N individuals distributed in a two-dimensional space with coordinates (a, b), it is possible to tabulate the frequency function $\Psi(a, b)$ by evaluating the observed local density at each node of a grid of $n_a \times n_b$ points extending over the region of interest in the space. If the grid is dense enough, the empirical frequency function $\{\Psi(a_i, b_j); i = 1, ..., n_a; j = 1, ..., n_b\}$ will be equivalent, for all practical purposes, to the true $\Psi(a, b)$. The kernel used to estimate that local density around a point (a_i, b_j) will be a normal circular kernel. The smoothing parameter h (Gaussian dispersion), is chosen using Silverman's rule (1986). The procedure was tested for several subsamples applying different proper motion cutoffs. Satisfactory results are obtained with a proper motion cutoff of $|\mu| \leq 15$ mas yr^{-1}.

The only assumptions we need to apply in the non-parametric approach in our case, are the following:

1. it is possible to select some spatial area in the region under study relatively free of cluster stars, and to determine the frequency function corresponding to the VPD of this area. This will provide a representation of the field frequency function with a small (or negligible) cluster contribution, and

2. the frequency function found this way is representative of the field frequency function over the whole plate and, specifically, in the area occupied by the cluster.

The empirical frequency function determined from the VPD corresponding to the area occupied by the cluster, Ψ_{c+f}, is made up of two contributions: cluster and

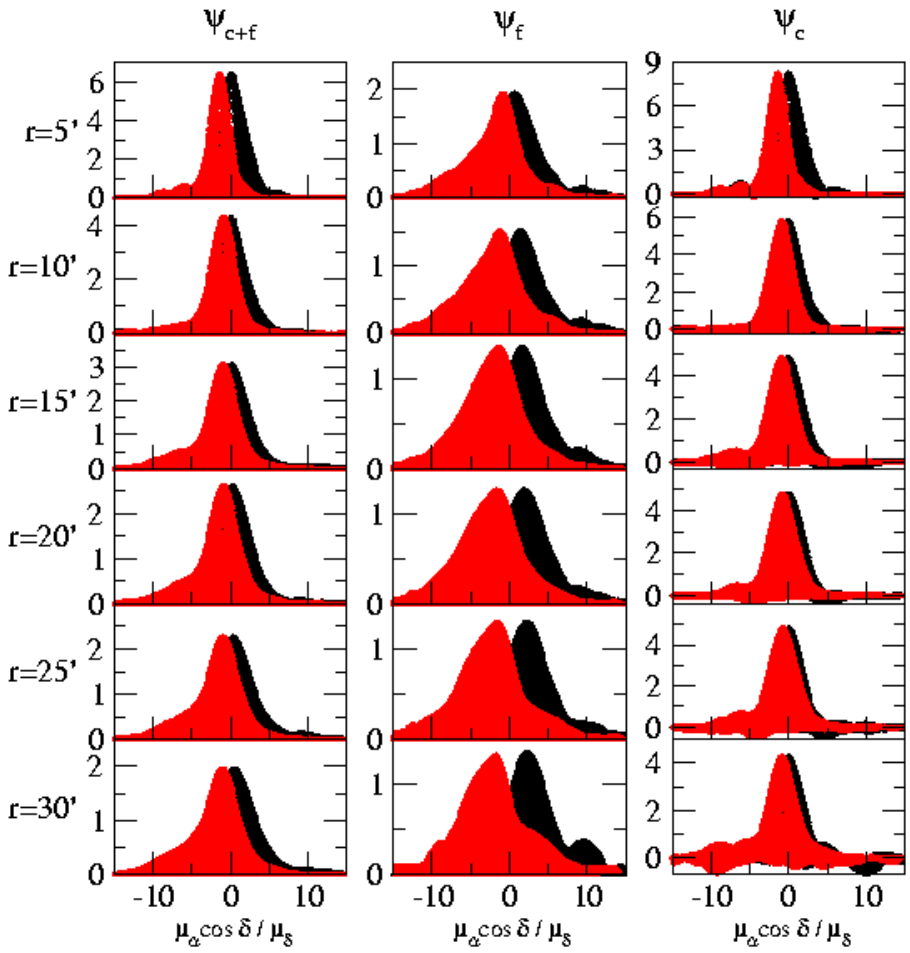

Figure 2.11: Empirical probability density functions for the mixed sample, ψ_{c+f}, the field population, ψ_f, and the cluster population, ψ_c, for NGC 1817 taking different radii, r. At the back $\mu_\alpha \cos\delta$ in black, at the front μ_δ in red.

field. To disentangle the two populations we need to estimate the field distribution. For this purpose, we studied the VPD for the plate area outside a circle centred on the cluster. The centre of the cluster was chosen as the point of highest spatial density. We did tests with circles of very different radii (see Figs 2.11 and Table 2.9), searching a reasonable tradeoff between cleanness (absence of a significant amount of cluster members) and signal-to-noise ratio (working area not too small). The kernel density estimator was applied in the VPD to these data, yielding the empirical frequency function, for a grid with cell size of 0.2 mas yr^{-1}, well below the proper motion errors.

We finally found that the area outside a circle with a radius of $20'$ centred on the cluster yields a clean frequency function with low cluster contamination and low noise. This way we deduce the frequency function representative of the field population. The next step was to determine Ψ_{c+f} from a plate area centred on the cluster and containing both populations (cluster and field). We found that in our case the inner circle with a radius of $20'$ is well suited for our purposes. Assuming that the spatial stellar density of the field population is approximately uniform over the whole area surveyed, we can scale the field frequency function previously computed to represent the field frequency function in the inner circle, Ψ_f, by simply applying a factor linked to the area. The cluster empirical frequency function can then be determined as $\Psi_c = \Psi_{c+f} - \Psi_f$. These empirical frequency functions can be normalised to yield the empirical PDFs for the mixed populations (inside the circle), for the field (outside the circle) and for the cluster (non-field) population. Figure 2.12 displays these three functions. The probability for a star in a node of the grid being a member of the cluster is $P_c = (\Psi_{c+f} - \Psi_f)/\Psi_{c+f}$. The empirical tables can then be used to estimate the probability of a star being a cluster member according to the probability of its nearest node. These probability tables are then applied to all the stars in the surveyed area, both inside and outside the circle defined to determine the functions.

Of course, the field PDF estimated in the outer area cannot be an absolutely perfect representation of the true field PDF in the whole area. This introduces undesired noise in the frequency function of the cluster. The negative density values found in several zones obviously lack physical meaning. These negative values allow us to estimate the typical noise level, γ, present in the result. To avoid meaningless probabilities in zones of low density we restricted the probability calculations to the stars with cluster PDF $\geq 3\gamma$. The maximum of the cluster PDF is located at

Table 2.9: Comparison of the position, maximum and FWHM of the empirical probability density function of the total, the field and the substracted cluster NGC 1817 taking different radii for the cluster area. The last column gives the FWHM for each component $(\mu_\alpha \cos\delta, \mu_\delta)$ and the averaged value.

r	$(\mu_\alpha \cos\delta)_{\rm c+f}$	$(\mu_\delta)_{\rm c+f}$	$(\psi_{\rm c+f})_{\rm max}$	$\mathrm{FWHM}_{\psi_{\rm c+f}}$
	$(\mu_\alpha \cos\delta)_{\rm f}$	$(\mu_\delta)_{\rm f}$	$(\psi_{\rm f})_{\rm max}$	$\mathrm{FWHM}_{\psi_{\rm f}}$
	$(\mu_\alpha \cos\delta)_{\rm c}$	$(\mu_\delta)_{\rm c}$	$(\psi_{\rm c})_{\rm max}$	$\mathrm{FWHM}_{\psi_{\rm c}}$
(arcmin)	(mas yr^{-1})	(mas yr^{-1})	-	(mas yr^{-1})
5	0.0±0.2	-1.4±0.2	6.4	3.6/3.0→3.3
	0.6±0.2	-0.8±0.2	1.9	5.2/5.2→5.2
	0.0±0.2	-1.4±0.2	8.3	3.4/2.8→3.1
10	0.0±0.2	-0.8±0.2	4.3	4.0/3.6→3.8
	1.4±0.2	-1.2±0.2	1.5	5.6/6.6→6.1
	0.0±0.2	-0.8±0.2	5.8	3.6/3.4→3.5
15	0.2±0.2	-1.0±0.2	3.1	4.6/4.0→4.3
	1.6±0.2	-1.4±0.2	1.3	6.0/7.2→6.6
	0.0±0.2	-1.0±0.2	4.9	3.8/3.8→3.8
20	0.2±0.2	-1.0±0.2	2.6	4.6/4.4→4.5
	2.0±0.2	-1.6±0.2	1.3	6.6/7.8→7.2
	0.0±0.2	-0.8±0.2	4.8	4.0/4.0→4.0
25	0.4±0.2	-1.0±0.2	2.3	4.8/4.6→4.7
	2.2±0.2	-1.6±0.2	1.3	6.4/7.4→6.9
	0.0±0.2	-0.8±0.2	4.8	4.0/4.2→4.1
30	0.4±0.2	-1.0±0.2	2.0	5.2/4.8→5.0
	2.2±0.2	-1.8±0.2	1.4	6.2/7.4→6.8
	0.0±0.2	-0.8±0.2	4.3	3.8/3.8→3.8

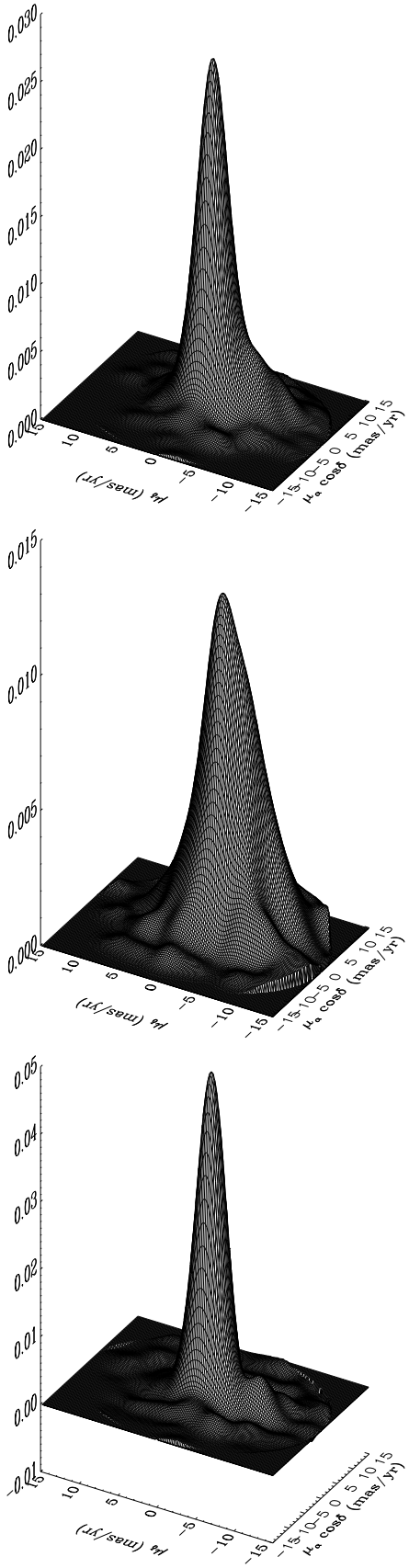

Figure 2.12: Empirical probability density functions in the kinematic plane. Top: ψ_{c+f} mixed sample from the inner circle of 20'. Centre: ψ_f field population from outside this circle. Bottom: ψ_c cluster population of NGC 1817

$(\mu_\alpha \cos\delta, \mu_\delta) = (0.0\pm0.2, -0.8\pm0.2)$ mas yr^{-1}.

Like the negative density values, the small local maximum found in the cluster PDF around $(\mu_\alpha \cos\delta, \mu_\delta) = (0.0, -6.0)$ mas yr^{-1} is also due to the fact that the empirical frequency function computed in the outer area of the plate does not represent the inner circle field frequency function with absolute accuracy. The stars with proper motions in this VPD area are spread over the plate and their photometry (when available from Chapter 3) does not suggest that they correspond to any physical group.

2.6.2.1 Effectiveness of membership determination

We can also apply Equation (2.11) to calculate the effectiveness of membership determination for the non-parametric approach. For NGC 1817 we found a value of $E = 0.52$. As pointed in Section 2.3.1.1, such a low value of E should be interpreted as a very low contrast between the cluster and field frequency functions. If the model used is suitable, as believed, this is a clear insight of the level of entangling of the two populations.

2.6.3 The non-parametric approach in the spatial plane

The kernel density estimator method was also applied to the selected sample in the spatial plane inside the circle centred on the cluster zone, with radius of $20'$. We set a grid of 221×221 nodes in both x and y coordinates. This gives a cell size of $16'' \times 16''$ that leads to an average stellar density of about 0.11 stars per cell. The resulting empirical frequency function Ψ^s_{c+f} (where "s" stands for "space") should be decomposed into field and cluster contributions: $\Psi^s_{c+f} = \Psi^s_c + \Psi^s_f$.

In order to estimate the field spatial density distribution we computed the spatial frequency function $\Psi^s_{f'}$ in the area outside the cluster zone, with radius $20'$, as we did in the kinematic plane. To extrapolate this frequency function to the inside circle, we fit a tilted plane to the distribution found in the corona. The tilt was found to be very slight, and this validates the assumption made in the previous section concerning the uniformity of the spatial stellar density of the field. This tilted plane was assumed to represent the spatial frequency function in the inner circle Ψ^s_f and

was subtracted from the mixed distribution.

The spatial PDF's ψ^s_{c+f}, ψ^s_c, ψ^s_f were obtained from the frequency function by normalizing to unit volume. The spatial probability of a star could be computed as: $P^s_c = (\Psi^s_{c+f} - \Psi^s_f)/\Psi^s_{c+f}$.

The resulting empirical spatial PDF is shown in Figure 2.13. The spatial distribution of the cluster is very extended and with a low contrast from the field. The two groupings standing out have been the reason for the introduction of two separate NGC entries in the classical literature. This plane shows not to be very meaningful and after several tries, we decided not to use it for our segregation of cluster and field.

2.6.4 Results and discussion

The results from the non-parametric and parametric approaches are in agreement, which indicates the reliability of both methods in the case of this cluster. While in the parametric approach we need to impose a null internal dispersion (based on the known distance of the cluster) for a reliable segregation, in the non-parametric approach we are able to disentangle the cluster population without the need of any a priori knowledge.

Furthermore, the parametric approach is quite sensitive to the initial values used for the iterations, and special care has to be taken at every step to ensure that the final results make sense from a physical point of view. In the case of a doubtful number of independent clusters present in an area the parametric method can be misleading (as happened in Section 2.3) and additional information has to be introduced explicitly to get the PDFs. On the contrary, as shown by Galadí-Enríquez et al. (1998a), if there is more than one cluster in a zone (and they show a distinctive kinematic behaviour), the non-parametric approach is capable of detecting and managing them in a direct and natural manner. In our case, we detected no sign of a distinct cluster NGC 1807 in the kinematic plane.

On the other hand, the non-parametric approach does not take into account the errors of the individual proper motions, therefore it does not make any particular distinction between bright or faint stars, different epoch spread and so on. The FWHM of the empirical cluster PDF provides an estimation of the errors of the dis-

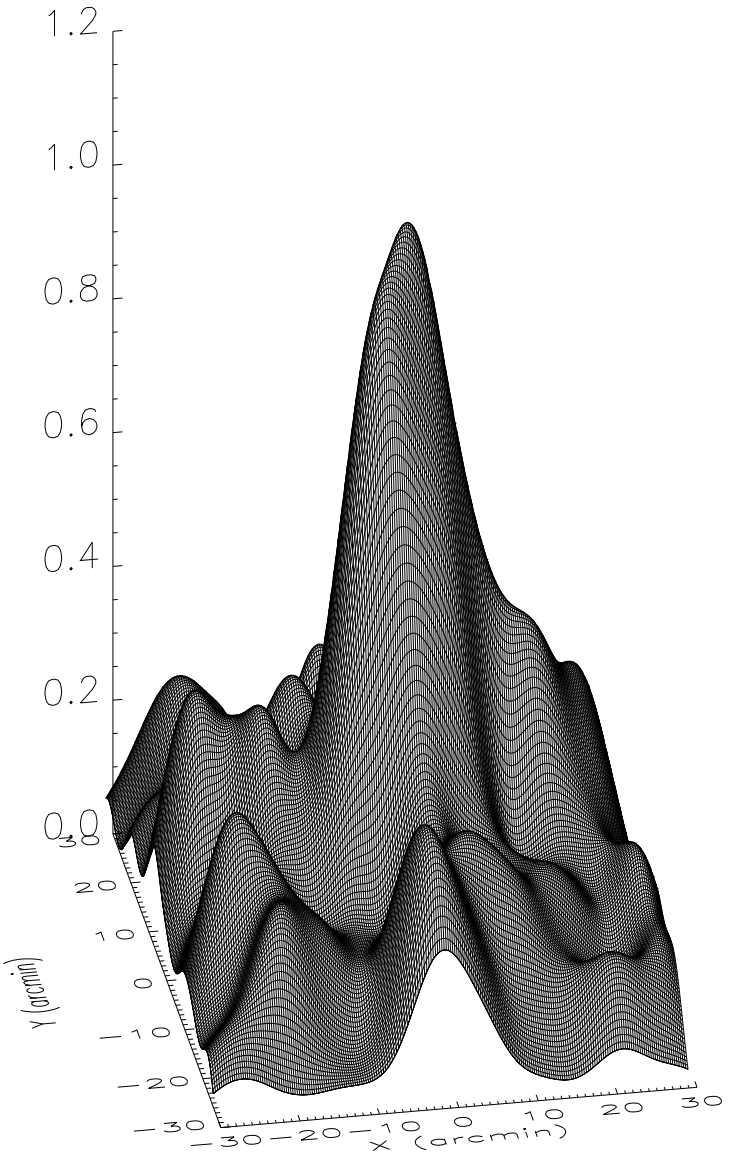

Figure 2.13: Empirical probability density function (ψ^s_{c+f}) in the spatial plane.

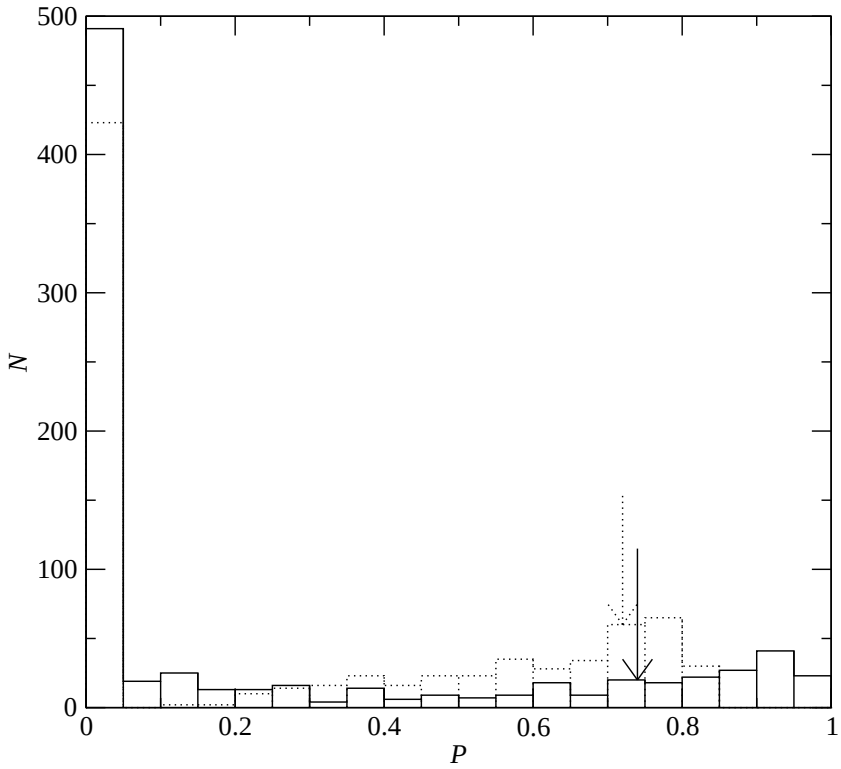

Figure 2.14: The histogram of cluster membership probability of NGC 1817. The solid line gives the results for traditional parametric method (Section 2.6.1), while the dotted line corresponds to the non-parametric approach (Section 2.6.2). The arrows mark the limiting probabilities adopted for member selection in each method.

tribution. We obtained a FWHM of $\sim$4.0$\pm$0.2 mas yr^{-1}. If the Gaussian dispersion owing to the smoothing parameter h = 1.33 mas yr^{-1} is taken into account, this FWHM corresponds to a mean error in the proper motions of 1.5 mas yr^{-1}, of the same order as the values given in Section 2.5.

The cluster membership probability histogram (Figure 2.14) shows a similar degree of separation between cluster members and field stars in both approaches: the solid line is the traditional parametric method while the dotted line is the non-parametric approach. But the exact point of deciding which probability means that a star is a member has been traditionally left to a usually conservative, but subjective, arbitrary decision (0.7 in Section 2.3). The non-parametric approach gives an expected number of cluster members from the integrated volume of the cluster frequency function Ψ_c in the VPD areas of high cluster density (where $\Psi_c > 3\gamma$). This integration predicts that the sample contains 135 cluster members. Sorting the sample in order of decreasing non-parametric membership probability, P_{NP}, the first 135 stars are the most probable cluster members, according to the results of the non-parametric technique. The minimum value of the non-parametric probability (for the 135-th star) is P_{NP} = 0.72.

There is no an equivalent rigurous way to decide where to set the limit among members and non-members in the list sorted in order of decreasing parametric membership probability, P_P. But, if we accept the size of the cluster predicted by the non-parametric method, 135 stars, we can consider that the 135 stars of highest P_P are the most probable members, according to the results of the parametric technique. The minimum value of the parametric probability (for the 135-th star) is P_P = 0.74.

With these limiting probabilities ($P_{NP} \geq 0.72$; $P_P \geq 0.74$), we get a 92% (743 stars) agreement in the segregation yield by the two methods. The 67 remaining stars (8%) with contradicting segregation should be carefully studied. Discrepancies among the two approaches are actually expected due to the statistical nature of the methods themselves.

Thus, we find ourselves with two lists of member candidates. To set up a final and unique list, and being conservative, we accept as probable members of this cluster those stars classified as members by at least one of the two methods. This is equivalent to merging both lists (each with 135 stars) and eliminating duplicated entries. This way we get a list of 169 probable member stars.

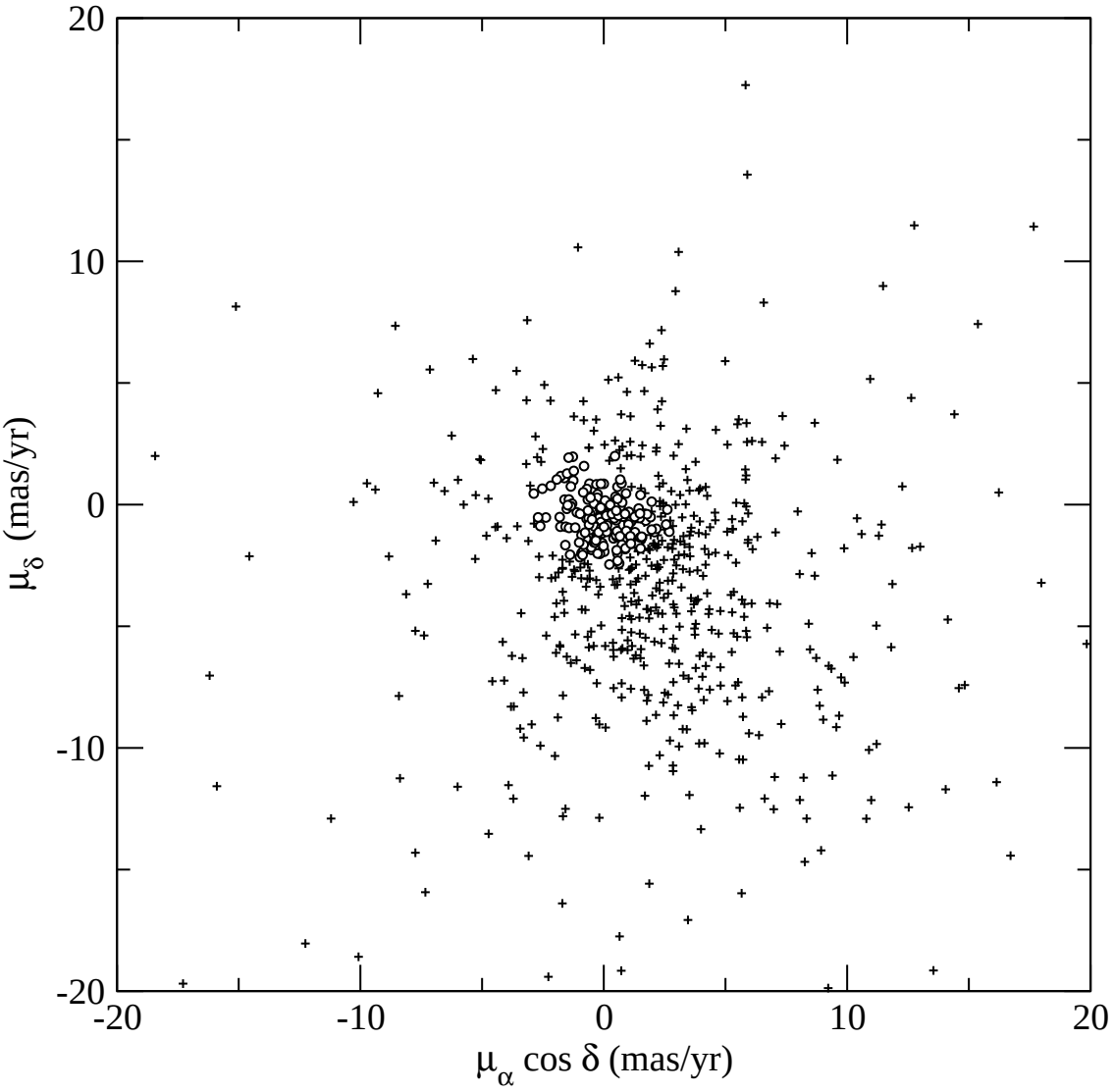

Figure 2.15: The proper motion vector-point diagram of stars in NGC 1817 ("○" for members of NGC 1817, "+" for field stars)

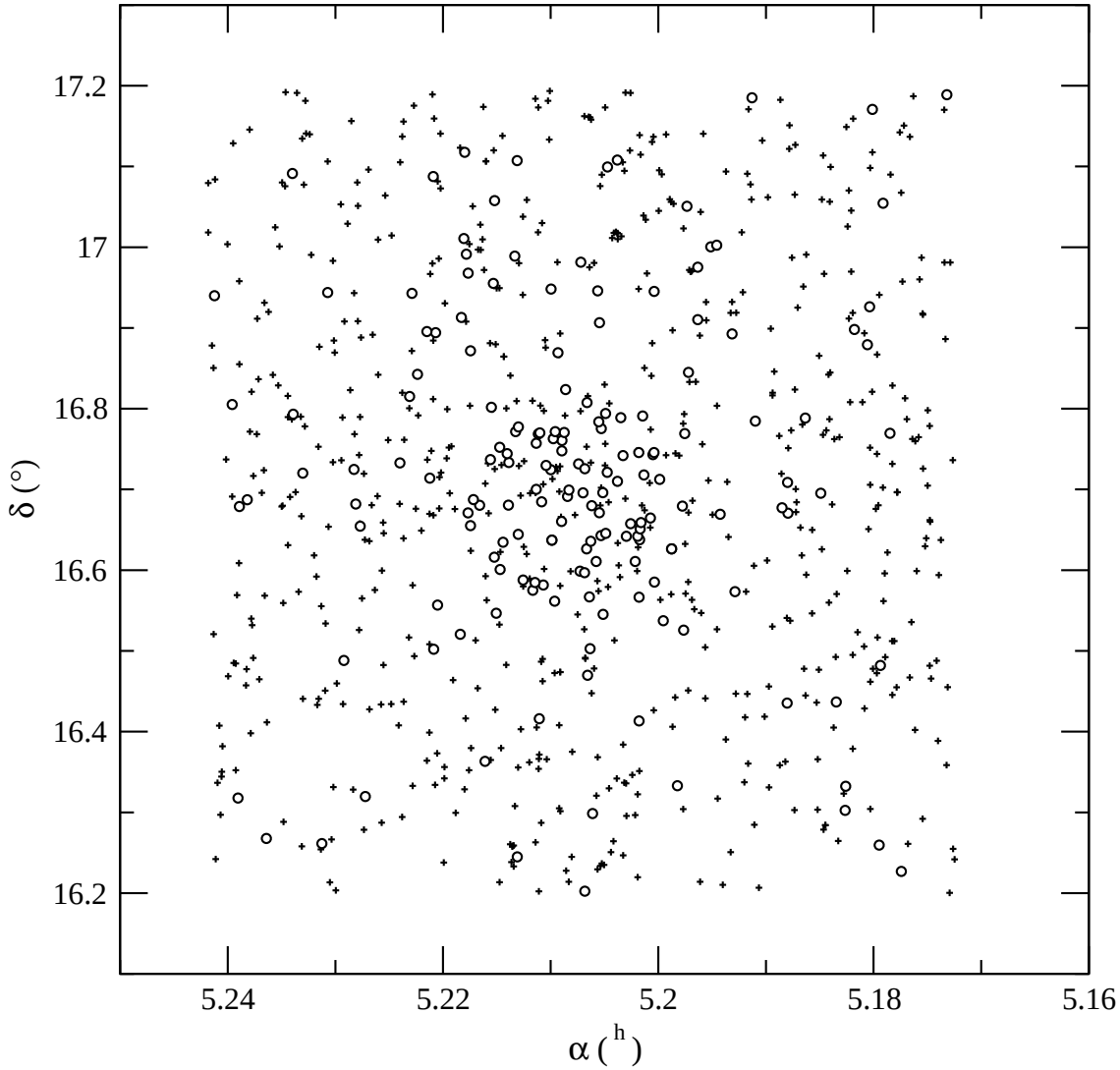

Figure 2.16: The position distribution of stars in NGC 1817 ("○" for members of NGC 1817, "+" for field stars)

As in any other cluster membership study based on kinematic information, the resulting list of probable members has to be complemented with additional information for a cleaner segregation (see Chapter 3).

In Section 2.3, 416 stars were considered members of NGC 1817 ($P_1 > 0.7$), while 14 stars were considered members of NGC 1807 ($P_2 > 0.7$). Only one of those 14 stars is a member of NGC 1817 now, and the rest belong to the field. A detailed comparison of the results here with those in Section 2.3 for NGC 1817 shows 113 members in common with the parametric segregation and 120 in common with the non-parametric one. Hence, Section 2.3 was overestimating the cluster population by as much as approximately 300 stars that most probably belong to the field.

Figures 2.15 and 2.16 show the proper motion VPD and the sky distribution for all the measured stars, where "$\circ$" denotes a selected member of NGC 1817, and all other stars are considered field stars indicated by "+".

A comparison with the 76 stars included in the radial velocity study by Mermilliod et al. (2003) is given in Table 2.12. The radial velocities have errors of ≈ 0.5 km s^{-1}. To quantify the differences we set an agreement index P_c to 1 if the parametric probability, P_P, agrees with the radial velocity segregation, 2 if the non-parametric probability, P_{NP}, agrees, 3 if both probabilities agree and 0 if none does. We find 62 out of 76 stars with $P_c > 0$, that is 82% agreement with the radial velocities segregation. 18% of the disagreement consists of 10 stars out of 36 (28%) being considered non-members on the basis of proper motions while only 4 out of 40 (10%) were found to be astrometric members while considered non-members on the basis of radial velocities.

If we compare the two methods, the behaviour is rather similar. For the parametric method we find a total of 60 stars (79%) whose membership assignation coincides with the radial velocity criterion, while for the non-parametric method this amounts to 54 stars (71%).

The results show that the two approaches are similar when the parameters are well established in the parametric method and when a suitable area free from cluster stars is chosen in the non-parametric technique. But we need to be aware of the risks of the parametric model when there is more than one cluster or probable cluster. We consider the non-parametric approach a good alternative to avoid mathematical artefacts.

Table 2.13[4] lists the results for all 810 stars in the region of the open cluster: column 1 is the ordinal star number (as in Section 2.3, the numbering system comes from the PDS measuring machine); columns 2 and 3 give $\alpha_{\rm J2000}$ and $\delta_{\rm J2000}$; columns 4 and 6 list the respective absolute proper motions ($\mu_\alpha \cos\delta, \mu_\delta$); columns 5 and 7 contain the standard errors of the proper motions; column 8 gives the number of plates used to derive proper motions; column 9 and 10 are the parametric and non-parametric membership probabilities of stars belonging to NGC 1817 and column 11 provides the identification number in the Tycho-2 Catalogue for the stars in common.

The present results for NGC 1817, based on astrometric data only, are complemented with the photometric study of Chapter 3.

[4]Table 2.13 is only available in electronic form at the CDS via anonymous ftp to cdsarc.u-strasbg.fr (130.79.128.5) or via `http://cdsweb.u-strasbg.fr/cgi-bin/qcat?J/A+A/426/819/`

Table 2.12: The cross-identification of stars in common with the radial velocities analysis by Mermilliod et al. (2003) and the comparison of its membership for parametric (P_P) and non-parametric (P_{NP}) results. See text for explanation of the agreement index P_c.

Id_M	$Id_{2.13}$	P_P	P_{NP}	P_c	P_{Vr}	Id_M	$Id_{2.13}$	P_P	P_{NP}	P_c	P_{Vr}
8	557	0.40	0.65	0	M	90	554	0.00	0.47	3	NM
12	562	0.88	0.77	3	M	103	580	0.01	0.28	3	NM
19	358	0.92	0.73	3	M	138	322	0.57	0.62	3	NM
22	351	0.70	0.66	0	M	155	519	0.08	0.78	1	NM
30	334	0.65	0.63	0	M	161	527	0.00	0.31	3	NM
40	541	0.85	0.80	3	M	187	394	0.00	0.00	3	NM
44	546	0.98	0.78	3	M	269	521	0.00	0.00	3	NM
56	379	0.96	0.79	3	M	531	432	0.00	0.35	3	NM
71	317	0.58	0.60	0	M	536	448	0.00	0.00	3	NM
72	318	0.73	0.81	2	M	571	610	0.81	0.81	0	NM
73	528	0.95	0.81	3	M	598	696	0.00	0.00	3	NM
79	543	0.94	0.77	3	M	621	768	0.00	0.00	3	NM
81	542	0.79	0.77	3	M	1081	885	0.00	0.00	3	NM
121	367	0.94	0.71	1	M	1082	886	0.00	0.78	1	NM
127	339	0.86	0.82	3	M	1083	896	0.00	0.00	3	NM
164	532	0.98	0.80	3	M	1095	870	0.88	0.77	0	NM
177	577	0.81	0.63	1	M	1096	863	0.00	0.34	3	NM
211	331	0.55	0.80	2	M	1112	733	0.72	0.62	3	NM
212	321	0.90	0.74	3	M	1153	815	0.00	0.23	3	NM
244	556	0.92	0.75	3	M	1161	811	0.00	0.00	3	NM
185	395	0.93	0.81	3	M	1194	674	0.00	0.00	3	NM
206	343	0.91	0.78	3	M	1197	672	0.00	0.30	3	NM
1114	735	0.79	0.70	1	M	1246	468	0.00	0.00	3	NM
1117	600	0.97	0.74	3	M	1248	467	0.15	0.54	3	NM
1135	714	0.90	0.82	3	M	1252	660	0.00	0.00	3	NM
1152	816	0.00	0.35	0	M	1254	648	0.00	0.44	3	NM?
1208	689	0.03	0.28	0	M	1267	237	0.00	0.00	3	NM
1265	463	0.19	0.51	0	M?	1273	112	0.00	0.00	3	NM
1292	605	0.87	0.65	1	M	1297	430	0.94	0.73	0	NM?
1408	301	0.97	0.76	3	M	1302	423	0.00	0.77	1	NM
1412	150	0.93	0.79	3	M	1314	206	0.00	0.00	3	NM
1420	160	0.75	0.75	3	M	1316	214	0.00	0.21	3	NM
1433	180	0.97	0.74	3	M	1406	304	0.93	0.78	0	NM
1456	292	0.69	0.68	0	M	1418	56	0.00	0.45	3	NM
1459	296	0.03	0.66	0	M	1424	3	0.00	0.27	3	NM
1574	65	0.05	0.52	0	M	1455	502	0.40	0.82	1	NM
						1467	493	0.00	0.00	3	NM
						1502	122	0.65	0.48	3	NM?
						1557	91	0.00	0.00	3	NM
						1718	162	0.00	0.00	3	NM?

Id_M: Identification number from Mermilliod et al. (2003).

$Id_{2.13}$: Identification number from Table 2.13